# Drosophila Tubulin-Specific Chaperone E Recruits Tubulin around Chromatin to Promote Mitotic Spindle Assembly

Mathieu Métivier, Emmanuel Gallaud, Alexandre Thomas, Aude Pascal, Jean-Philippe Gagné, Guy G. Poirier, Denis Chrétien, Romain Gibeaux, Laurent Richard-Parpaillon, Christelle Benaud, et al.

Version of Record: https://www.sciencedirect.com/science/article/pii/S0960982220316845
Manuscript_4d7141621656015f13a6e7057d25a137

# *Drosophila* Tubulin-specific Chaperone E recruits tubulin around chromatin to promote mitotic spindle assembly

Mathieu Métivier[1], Emmanuel Gallaud[1], Alexandre Thomas[1], Aude Pascal[1], Jean-Philippe Gagné[2], Guy G. Poirier[2], Denis Chrétien[1], Romain Gibeaux[1], Laurent Richard-Parpaillon[1], Christelle Benaud[1], and Régis Giet[1*]

[1] Univ Rennes, CNRS, IGDR (Institut de Génétique et Développement de Rennes) - UMR 6290, F-35000 Rennes, France

[2] Centre de Recherche du Centre Hospitalier Universitaire de Québec - Pavillon CHUL, Université Laval, Québec, QC, Canada.

[*] Corresponding author: regis.giet@univ-rennes1.fr

Lead Contact: Régis Giet

**Summary**

Proper assembly of mitotic spindles requires microtubule nucleation not only at the centrosomes but also around chromatin. In this study, we found that the *Drosophila* tubulin-specific chaperone dTBCE is required for the enrichment of tubulin in the nuclear space after nuclear envelope breakdown and for subsequent promotion of spindle microtubule nucleation. These events depend on the CAP-Gly motif found in dTBCE, and are regulated by Ran and lamin proteins. Our data suggest that during early mitosis, dTBCE and nuclear pore proteins become enriched in the nucleus, where they interact with the Ran GTPase to promote dynamic tubulin enrichment. We propose that this novel mechanism enhances microtubule nucleation around chromatin, thereby facilitating mitotic spindle assembly.

## Introduction

Microtubules (MTs) are essential dynamic components of the cytoskeleton that assemble from α- and β-tubulin dimers [1]. During cell division, the MT cytoskeleton is remodelled to assemble a MT-based bipolar spindle. This ensures the accurate attachment of sister chromatids with the opposite spindle poles, and allows their equal segregation toward the daughter cells. *In vitro*, MT nucleation occurs spontaneously in the presence of GTP when a critical concentration of tubulin dimers is reached. In somatic cells, the nucleation of mitotic spindle MTs requires several additional factors and occurs both at centrosomes and around mitotic chromatin. MT-nucleating proteins include the γTuSC gamma-tubulin small complex, which targets the centrosome and pre-existing MTs [2, 3, 4, 5]. Around chromatin, MT nucleation is triggered by a Ran-GTP gradient that allows for the local release of spindle assembly factors (SAFs) sequestered by importins [6]. However, the Ran pathway is not essential for MT nucleation in some model organisms [7, 8]. Indeed, the chromosomal passenger complex (CPC) also contributes to MT nucleation, and it can compensate for an absence of Ran [9,10.] Yet, even if *in vitro* MT nucleation was known to depend on tubulin concentration, it is only recently that local accumulation of free tubulin has been considered a key element that may have a significant contribution to spindle assembly [11, 12]. Interestingly, in both *Caenorhabditis elegans* and *Drosophila melanogaster,* an accumulation of free tubulin around centrosomes and chromosomes has been observed during mitosis, although the physiological relevance of this local tubulin increase is not completely understood [11, 13-15].

Tubulin-binding co-factors exist as five proteins (TBCA to TBCE) whose concerted action leads to the assembly of polymerization-competent tubulin heterodimers [16]. However, whether these proteins have independent and/or additional functions remains an open question. We previously identified the *D. melanogaster* tubulin-binding co-factor E (dTBCE) as a protein with a putative mitotic function, since knockdown of the protein produces abnormal mitosis in brain neuroblasts (Nbs) [17]. Here, we demonstrate that dTBCE is responsible for the recruitment of tubulin around chromatin during prophase, and that this mechanism is essential for proper spindle assembly.

## Results

### Both dTBCE localization and fly viability depend on the presence of the chaperone's conserved CAP-Gly motif

The dTBCE protein was previously isolated from Taxol-stabilized MT pellets from early mitotic embryos, suggesting that it may have an affinity for the mitotic spindle [17, 18] . To investigate the localization of dTBCE during mitosis, we used the GAL4/UAS system to generate transgenic flies expressing wild-type dTBCE tagged with GFP under the control of the V32-GAL4 maternal promoter (Figure 1B and Video S1). In early dividing embryos, dTBCE-GFP was present both in the cytoplasm and in the nucleus, with a pool of proteins clearly apparent on the nuclear envelope and on centrosomal MT asters (Figure 1B, arrows, Video S1, and Figure S1A). During nuclear envelope breakdown (NEBD), dTBCE-GFP was rapidly enriched in the nuclear space (Figure 1B, time 12:30). During metaphase, dTBCE decorated the mitotic spindle region (Figure 1B, time 14:30), and it remained on the MTs in anaphase (Figure S1A, time 16:00). dTBCE harbours a highly conserved N-terminal cytoskeleton-associated protein-glycine-rich (CAP-Gly) motif (Figure 1A, top left). This domain is known to mediate protein/protein interactions, including binding to the α-tubulin C-terminal tail [19, 20]. The functional importance of this CAP-Gly motif has been further suggested by the identification of a deletion of four amino acids immediately downstream of this motif in the genotype of human patients suffering from Hypoparathyroidism-retardation-dysmorphism (HRD) syndrome (Figure 1A, bottom left) [21] . In addition, dTBCE displays a putative weak nuclear localization signal (NLS) in its C-terminal ubiquitin-like domain (UBL) (Figure 1A, bottom right). To investigate the importance of these two motifs, we generated several dTBCE mutants then performed live analysis of their distributions as well as their ability to rescue *dtbce* mutant lethality (see Methods). To fully disrupt the functionality of the CAP-Gly domain, we mutated the two most conserved residues of the motif (dTBCE$^{mutCG}$) (Figure 1A, top right). In parallel, we also deleted the four amino acids following that motif to mimic the mutation observed in HRD patients (TBCE$^{HRD}$-GFP) (Figure 1A bottom left). Finally, we also mutated the putative NLS (TBCE$^{mutNLS}$) (Figure 1A bottom right). We noticed that both dTBCE-GFP and dTBCE$^{HRD}$-GFP were able to fully restore *dtbce* viability (100% rescue, $n$ > 100 flies per construct, 3 transgenes tested). In contrast, three independent transgenic lines expressing either dTBCE$^{mutCG}$-GFP or dTBCE$^{mutNLS}$-GFP were not able to rescue the *dtbce* lethality (0% rescue, $n$ > 100 flies per construct). We then used a maternal driver to monitor the live-embryo localizations of

dTBCE$^{mutCG}$-GFP (Figure 1C, Video S2, and Figure S1B), dTBCE$^{HRD}$-GFP (Figure 1D, Video S3, and Figure S1C), and dTBCE$^{mutNLS}$-GFP (Figure 1E, Video S4, and Figure S1D). Western blot analysis revealed that dTBCE-GFP and dTBCE$^{mutNLS}$-GFP proteins were expressed at similar levels, but that both dTBCE$^{HRD}$-GFP and dTBCE$^{mutCG}$-GFP were less abundant, suggesting that the integrity of the CAP-Gly domain may affect protein stability (compare lanes 3 and 6 to lanes 4 and 5 in Figure S2). Strikingly, the dTBCE$^{mutCG}$-GFP protein did not associate with the nuclear envelope during interphase or with the centrosomal MT asters or mitotic spindle, and instead displayed a uniform cytoplasmic distribution (Figure 1C, Video S2, and Figure S1B). Neither the deletion adjacent to the CAP-Gly motif observed in HRD patients (Figure 1D, Video S3, and Figure S1C) nor the mutation of the putative NLS/UBL strongly impaired the localization pattern of these dTBCE variants (Figure 1F, Video S4, and Figure S1E). These data suggest that the highly conserved amino acids in the CAP-Gly domain play a key role in dTBCE functionality and dynamics. Furthermore, while the CAP-Gly motif is absolutely essential for fly viability, its deletion (as in the mutation observed in HRD patients) does not alter its ability to rescue the *dtbce* mutation, nor does it strongly alter the dynamics of the corresponding proteins. Finally, although the abrogation of the putative NLS located in the conserved UBL did not strongly impair the protein's dynamics or its ability to be enriched in the nuclear space during mitosis, this variant failed to rescue the *dtbce* mutant. This suggests that it is the integrity of the UBL rather than the existence of an NLS that is responsible for dTBCE functionality.

**dTBCE associates with nuclear pore proteins and components of the Ran pathway through the CAP-Gly motif**

To deepen our molecular understanding of dTBCE functioning, we set out to identify any interacting partners whose interactions depend on a functional CAP-Gly motif. To do this, we generated S2 stable cell lines expressing GFP, GFP-tagged dTBCE, and dTBCE$^{mutCG}$, then performed immunoprecipitation with anti-GFP nanobodies to check for the presence of proteins (see Methods and Figure 2A). In order to identify the proteins that interact with dTBCE but not with dTBCE$^{mutCG}$ or GFP, these immunoprecipitates were then subjected to proteomic analysis (Methods and Figure 2B and C). We found that dTBCE displayed a strong CAP-Gly-dependent association with nuclear pore proteins (NUPs) and members of the Ran pathway, including α- and β-importins as well as Ran itself, suggesting that dTBCE has a function up- and/or downstream of RAN (Figure 2B and C). To confirm the interaction of dTBCE with RAN *in vivo*, we prepared protein extracts from syncytial embryos expressing

GFP, dTBCE-GFP, or dTBCE$^{mutCG}$-GFP, then performed immunoprecipitation experiments. As seen with the S2 cells, these experiments confirmed that dTBCE-GFP interacts with both Ran and α-tubulin, and that in early embryos the strength of these interactions is dependent on the CAP-Gly motif (Figure 2D). To compare the localization of TBCE-GFP with components of the Ran pathway, we imaged early embryos expressing Ketel-GFP (importin-β) and Venus-Ran. Similarly to previous studies [22, 23] , we found that these two proteins display a nuclear association and were associated with the nuclear membrane during interphase. During mitosis, both Ketel and Ran were enriched in the mitotic spindle region (Figure S3A and B, times 8:30 and 2:30 respectively). For comparison, we also monitored the localization of another tubulin co-factor under the same conditions: dTBCD [24]. We discovered that dTBCD-GFP behaved like a cytoplasmic protein during cell division (Figure S3C). Finally, the gene ontology classification of the dTBCE-interacting proteins highlights the fact that these proteins are located at the boundary between the nuclear space and the cytoplasm, and their function are associated with the nucleocytoplasmic transport and with microtubules (Figure 2E). With the results of our biochemical and live imaging experiments, we can conclude that dTBCE is at the interface between tubulin and the Ran pathway.

**Lowering dTBCE levels impairs brain growth and triggers spindle assembly defects associated with a SAC-dependent mitotic delay**

dTBCE was initially described in a screen for genes that might be required for the mitotic spindle assembly of larval brain Nbs [17]. Because of the protein's localization pattern and interactions with Ran, a protein that plays a major role in the nucleation of spindle MTs around chromatin, we decided to carefully examine dTBCE-dependent mitotic spindle assembly defects. We therefore knocked down dTBCE in the fly central nervous system via a two-day treatment with two *dTBCE* UAS-driven dsRNA lines ('KK' and 'GD', see Methods), alone and combined. While the knockdown of the tubulin-binding co-factor dTBCD results in decreased tubulin levels [25], we found that RNAi-driven downregulation of dTBCE with one or two dTBCE-specific dsRNAs had no effect on the protein levels of α- or β-tubulin (Figure 3A). Strikingly, following two or three days of treatment with the double *dTBCE* RNAi, brain lobe diameters were respectively 6 and 10% smaller than those of the controls, indicating neural tissue growth defects (Figure 3B). In brain squash preparations, the chromosomes of dTBCE-depleted brains cells were frequently over-condensed, a phenotype characteristic of prolonged mitosis (Figure 3C) [26]. In agreement with these observations, mitotic index analysis revealed that knockdown of dTBCE with a single or pair of dsRNAs triggered significant

two-fold and four-times elevation in their respective mitotic indices (Figure 3D). Subsequent fixation of brain tissues and tubulin-staining revealed that the dTBCE-depleted Nbs exhibited strongly decreased MT densities within the spindle region during metaphase (Figure 3E, compare left and right). To quantify the mitotic defects in dTBCE-knockdown Nbs, we analysed cell division by live microscopy in cells expressing tubulin-GFP (Figure 3F). We found that the spindles of the dTBCE-knockdown Nbs were significantly shorter than those of the controls (Figure 3G). Interestingly, while mitotic duration at 29 °C was 5 min in the controls, knockdown of dTBCE by a single or a double RNAi treatment led to significant increases in mitotic timing (Figure 3H). Finally, the tubulin signals within the middle region of the metaphase spindles was decreased significantly, suggesting spindle assembly defects (Figure 3F, bottom row, arrowheads at 3:00 and 5:00, and Figure 3I). Mitotic delays and spindle abnormalities are frequently associated with spindle assembly checkpoint (SAC) activation. To examine the contribution of SAC to the mitotic delay observed in dTBCE-deficient cells, we began by analysing the mitotic indices of Nbs subjected to RNAi for the SAC gene *Mad2*, *dTBCE,* or the two together (Figure S4A and B). We noticed that double knockdown of Mad2 and dTBCE led to the disappearance of mitotic cells, over-condensed chromosomes, and the appearance of aneuploid cells (Figure S4A, arrowhead). In addition, the mitotic index (which was 2.39 ± 0.35% in dTBCE-knockdown neural tissues) dropped to 0.75 ± 0.11% in both dTBCE and Mad2-knockdown Nbs (Figure S4B). By analysing the mitotic timing of *dTBCE* RNAi-treated Nbs in the presence or absence of *Mad2* dsRNA (Figure S4C and D), we found that there was a complete rescue of mitotic timing when both Mad2 and dTBCE were knocked down. Finally, in fixed preparations we frequently detected lagging chromosomes in anaphase cells when both of these proteins were knocked down. This indicates that the SAC is required for maintaining genome stability in cells with low dTBCE levels, which is in agreement with the presence of aneuploid cells in that context (Figure S4A and E). Taken together, our data indicate that dTBCE is essential for proper mitotic spindle assembly in neural stem cells, and that it is required for normal larval brain growth.

**dTBCE is essential for the polymerization of mitotic spindle microtubules**

To investigate the origin of the low MT densities observed in the spindle region of dTBCE-deficient cells, we began by analysing MT regrowth at 25 °C after full cold-induced MT depolymerization (Figure 4A), as we have previously described [17]. In control cells, strong MT regrowth was observed after 30 s around the chromosomes (Figure 4A, arrowhead) and centrosomes. In addition, the mitotic spindles displayed a normal bipolar structure after only

90 s (Figure 4B, row 3). In contrast, in the dTBCE-knockdown cells we observed a severe impairment of MT nucleation on the kinetochores and spindle region after 30 s at 25 °C, while nucleation at the centrosome appeared similar to the control (Figure 4B, column 5). After 90 s, the *dTBCE* RNAi mitotic Nbs still showed this low-MT density on the spindle region (Figure 4B, column 6). Analysis of the mean spindle/centrosomal tubulin fluorescence ratio revealed a significant decrease in MT presence around chromatin in dTBCE knockdown cells 30 s after returning to 25 °C (Figure 4C).

We next decided to analyse and quantify MT nucleation in space and time in intact flattened metaphase Nbs by live tracking EB1-GFP proteins, which bind to MT plus ends (Figure 4D and E). For the controls, time projections and kymographs revealed that MT nucleation and elongation occurred both at the centrosomes (Figure 4D, arrows) and very strongly in the spindle region itself (Figure 4D and Video S5). In dTBCE-knockdown Nbs, MT nucleation at the centrosome was similar to the controls, but was clearly diminished in the spindle region, which suggests that MT nucleation was impaired around chromatin (Figure 4D and Video S6). Quantification of the EB1-GFP intensity signal ratio between the chromosomal region and the centrosome revealed a 50% decrease between the control and dTBCE-depleted mitotic Nbs (Figure 4E, $P < 0.0001$), while total EB1-GFP protein levels remained stable in both control and *dTBCE* RNAi-treated cells (Figure 4F). Together, these results show that the nucleation of microtubules and/or MT rescue around chromatin relies on dTBCE.

**Both Ran and dTBCE are required for tubulin enrichment and diffusion in the nuclear space during mitosis**

In agreement with previous studies [27-29], our data support the direct interaction of dTBCE with tubulin (Figure 2D). In addition, we found that dTBCE interacts with Ran GTPase, and that both proteins are required for the nucleation of MTs around chromatin (Figure 4) [6]. Upon entering mitosis, tubulin enrichment in the nuclear space is known to take place in *Drosophila* S2 and human HeLa cells, in *Drosophila* and worm embryos [13-15]. Interestingly, in *C. elegans* this event has been shown to be under the control of Ran [13]. We wondered therefore whether fly Nbs have a similar tubulin-enrichment mechanism in their nuclear space during mitotic entry. Because the MT tubulin signals is strong at the centrosomes and MT polymerization dynamics are rapid, tubulin enrichment in the nuclear space may be masked, so we depolymerized the MT network by incubating the tissue with colchicine (see Methods and Figure 5A). Under these conditions, we observed an accumulation of tubulin in the nucleus of the control, reaching a maximum intensity after 2 min (Figure 5B, top row, and Figure 5C and

D, grey curves). In *Ran* RNAi Nbs, the intensity of the increase in the nuclear-region tubulin signal was low and slow (Figure 5B, bottom row, and Figure 5C and D, orange curves). This indicates that when Ran is absent, tubulin has a hard time reaching the nuclear space. Similarly, when dTBCE was knocked down, the entry of tubulin into the nuclear space was decreased and slower (Figure 5B, middle row, Figure 5C and D, blue curves, and Figure 5F). In all three Nb types, increased tubulin in the nuclear space was always accompanied by decreased tubulin in the cytoplasm (Figure 5E). It was previously shown that tubulin diffusion and enrichment in the nuclear space in the one-cell *C. elegans* embryo is inhibited by the presence of nuclear lamins. To see whether this mechanism is conserved, we knocked down lamin in brain tissues for four days, at which point it was barely detectable in fixed Nb preparations (Figure 6A) and nuclear lamin signal quantification in individual Nbs revealed a strong knockdown (Figure 6B). Under these conditions, we observed a significant acceleration of tubulin entry into the nuclear space during early mitosis (Figure 6C and D). Thus, similarly to *C. elegans* embryos, the integrity of the lamina is essential for preventing premature tubulin enrichment in the nuclear space during early mitosis (Figure 6E).

**Dynamic tubulin-dTBCE interactions during early mitosis**

To investigate how dTBCE might be involved in tubulin enrichment in the nuclear space, we first monitored the dynamics of both Cherry-α-tubulin and dTBCE-Venus in that region in brain Nbs (Figure S5A). We treated the Nbs with colchicine and found that dTBCE was enriched there before tubulin (Figure S5B). This observation that dTBCE and tubulin entry in the nucleus were not concomitant supports the idea that instead of moving along with tubulin, dTBCE is enriched first in the nucleus. To verify dTBCE's capacity for dynamically bind tubulin, we immunoprecipitated and immobilized GFP, dTBCE-GFP, and dTBCE$^{mutCG}$-GFP on beads (see Methods), then assayed the ability of these beads to interact dynamically with purified tubulin-rhodamine (Figure 7A to C). We found that all three proteins were present at similar levels at the surface of the beads (Figure 7A and B). However, only the beads coated with dTBCE-GFP were able to efficiently bind to pure tubulin (Figure 7A and C). Interestingly, fluorescence recovery after photobleaching (FRAP) analysis revealed a continuous exchange between the bound and free tubulins in the bleached region (Figure 7D and E), indicating that the binding of the tubulin pool at the surface of the beads is fast and reversible. These experiments support the existence of a mechanism by which dTBCE is enriched in the nuclear space, which in turn creates a dynamic tubulin enrichment milieu that is required for spindle assembly (Figure 7F).

## Discussion

### dTBCE interacts with Ran and tubulin

Although differences exist between model systems, several decades of *in vitro* and *in vivo* studies have agreed that tubulin-binding co-chaperones contribute to the dynamics of microtubules [16, 30]. The common view is that the manipulation of tubulin chaperone levels in *Drosophila* and mammalian cells triggers defective MT polymerization because of an overall depletion in tubulin [21, 25, 31-34]. However, in agreement with some previous genetic studies of *Drosophila* and *Saccharomyces cerevisiae* [31, 35], we show here that low dTBCE levels are sufficient for sustaining normal tubulin levels but not for correct mitotic spindle assembly. As in a previous *Drosophila* experiment [32], our proteomic analysis using a functional dTBCE-GFP transgenic protein did not reveal any detectable interactions with other co-chaperones. Thus, even if co-chaperones when produced and manipulated *in vitro,* can assemble in a stable protein complex [16, 28], it is possible that it is unstable *in vivo*, present only at low levels *in vivo*, or assembled only under particular stress conditions as has been suggested by deletion studies in budding yeast [35]. One of the unexpected results of our study came from the analysis of the dTBCE interactome, where we saw that dTBCE has robust physical interactions with many nuclear pore proteins (Nups) and components of the Ran pathway, including Ran itself and importins (Figure 2). Another new and unexpected dTBCE feature came from the study of its dynamic localization. We see dTBCE on centrosomal MTs and the mitotic spindle. Moreover, and in agreement with its interaction with NUPs and Ran, we also found a pool of dTBCE that is associated with the nuclear membrane during interphase, enriched in the nucleus at the time of nuclear envelope breakdown, and then remaining in the spindle region during cell division (Video S1). This localization is different than that of other *Drosophila* tubulin chaperones, including dTBCD (Figure S3C) and dTBCB [32, 33]. Instead, our observations of dTBCE-GFP revealed that its localization resembles that of Ran and β-importin (Figure S3A and B) [22, 23]. We show that dTBCE's conserved CAP-Gly motif is necessary for its dynamic localization, for restoring the viability of *dtbce* null mutants, for mediating the protein's interaction with NUPs and the Ran machinery, and for tubulin interactions. Since the interaction of dTBCE with most of its binding partners is dependent upon the presence of this CAP-Gly motif, and as the motif is relatively small, it is tempting to speculate that these interactions are mutually exclusive, which would explain why dTBCE enters the nucleus first, before binding to tubulin. Interestingly, we were not able to find phenotypes associated with a dTBCE mutant mimicking the HRD human-disease variant

having a deletion of four amino acids upstream of the CAP-Gly motif. This is presumably because the shortness of the fly lifespan means that the protein retains enough of its functionality, and maybe more complex behavioural tests would be necessary to analyse possible defects. Finally, dTBCE does not harbour a functional nuclear localization signal, so it is not regulated as a true Ran NLS-containing target that is a nuclear protein during interphase.

**dTBCE-dependent tubulin enrichment in the nuclear space is required for normal mitotic spindle assembly**

Interestingly enough, dTBCE knockdown leads to the formation of shorter mitotic spindles with low MT densities. This mitotic phenotype as well as dTBCE's physical interactions with both tubulin and the Ran GTPase (a key regulator of chromatin-mediated MT nucleation) are interesting: in *C. elegans* embryos, tubulin enrichment process in the nuclear space is regulated by Ran, and it has been proposed to participate in mitotic spindle assembly [13]. This process has probably been underestimated as it is difficult to visualize "soluble" tubulin enrichment during early mitosis, in the presence of large centrosomes that concentrate high levels of tubulin nucleate numerous MTs at their surface. However, tubulin enrichment in the nuclear space is visible during NEBD in human cells and in *D. melanogaster* and *C. elegans* under MT depolymerising conditions [13-15]. We confirm here that a similar tubulin enrichment pathway is also present in the stem cells of the *Drosophila* central nervous system. Lowering dTBCE levels impairs this process, resulting in weakening of MT nucleation around chromatin and spindle assembly defects. Observation of tubulin and dTBCE dynamics in Nbs and embryos has shown that dTBCE is enriched before tubulin in the nuclear space, revealing that these two proteins do not "travel" together. Tubulin heterodimers are larger, and the size difference may be enough to cause the quicker enrichment of dTBCE in the nucleus, as suggested by a recent study [14]. However, given the strong association of dTBCE with nuclear pore proteins, and their similar dynamics, we propose that during prophase dTBCE and NUPs are reorganised together in the nuclear space to create a dynamic tubulin-interacting milieu. In agreement with this, our *in vitro* data show that dTBCE-GFP beads are able to concentrate and exchange tubulins. Such tubulin enrichment and turnover are likely essential for providing a reservoir of free tubulin available for the polymerization of spindle microtubules. Of note, we find that dTBCE-GFP beads are not sufficient to trigger nucleation, which suggests that other MT nucleation factors are needed to form a full MT nucleation pathway. One important result of our study is the observation of the physical interaction of dTBCE with

members of the RAN pathway who play important roles in mitosis and meiosis in many systems [6]. Ran also controls tubulin import into the nucleus in a similar manner as dTBCE (this work, [13]). dTBCE does not harbour a functional nuclear localization signal (Figure 1 and S1). In addition, nuclear pores are dismantled during early mitosis and fenestrated nuclear membranes persist around the spindle [36, 37]. Therefore, dTBCE cannot be imported into the nucleus by the Ran machinery. Instead, we hypothesize that Ran leads a reorganization of the nuclear space to create an environment conducive to tubulin enrichment, with subsequent nucleation and polymerization of spindle MTs (this paper [13, 38, 39]).

**Control of local tubulin concentrations as non-conventional MT-nucleation pathways**

The accumulation of tubulin in the nuclear space is driven by an organelle-exclusion mechanism. Indeed, laser ablation and mathematical modelling have suggested that the cytoplasm is a more crowded environment than the nucleoplasm. It has therefore been proposed that permeabilization of the nuclear membranes during early mitosis is sufficient for driving the accumulation of small molecules like tubulin and Mad2 into the nuclear space [14]. This mechanism is not selective, so theoretically any small cytoplasmic molecule could be enriched in the nucleus when the nuclear envelope breaks down. In order to locally and selectively allow tubulin enrichment in the nuclear space, there must therefore be a complementary pathway. We speculate that the dTBCE-dependent mechanism associates with the organelle-exclusion mechanism to regulate nuclear tubulin localization. Interestingly, knockdown of lamin significantly accelerated tubulin enrichment in the nuclear space during early mitosis (Figure 6). Therefore, similarly to what happens in one-cell *C. elegans* embryos, the integrity of the lamina contributes to maintaining the nuclear membrane as well prevention of premature tubulin entry [13]. We see several possible advantages to accumulating tubulin in the spindle region. First, we think that an accumulation of tubulin in the nuclear space of the nascent spindle region is particularly beneficial for cells with nuclei of large volume, such as Nbs. A simple prediction of such a high nucleus-to-cell size ratio is an overall dilution of tubulin concentration in prophase, leading to a less efficient MT nucleation. Secondly, the nuclear space is not an environment that favours the fast diffusion of tubulin without Ran or dTBCE (Figure 5C and D) [13]. Consequently, in the absence of a specialized mechanism to allow specific tubulin enrichment (or at least that facilitate a fast diffusion into the nuclear space), these two constraints limit MT nucleation around chromatin. In agreement with this hypothesis, preventing fast tubulin entry delays kinetochore capture and triggers activation of the spindle assembly checkpoint. Suppression of the SAC in dTBCE

knockdown cells leads to chromosome segregation defects, suggesting that tubulin enrichment is crucial for genome stability. Interestingly, TBCE is also required for MT nucleation in other subcellular compartments. For instance, MmTBCE is recruited to the Golgi apparatus and required for nucleation of Golgi-derived MTs, although it is not clear in this case whether the chaperone triggers local tubulin enrichment in order to mediate MT nucleation [40, 41]. In recent studies, it has been suggested that the mitotic centrosome is an organelle that can locally enrich tubulin through centrosomal microtubule-associated proteins (MAPs) [11, 12]. Congruently, inclusion of tubulin-binding proteins/MAPs in liquid droplets is sufficient for MT nucleation, raising the possibility that the local accumulation of tubulin-binding proteins is sufficient to concentrate tubulins and to build the "MT nuclei" required for the subsequent nucleation step [3]. An interesting question to explore will be whether local increases in tubulin concentrations that are promoted by proteins harbouring tubulin-binding motifs might be part of a more general mechanism involving the spatiotemporal regulation of microtubules.

## Acknowledgments

This work was supported by the Ligue Nationale contre le Cancer, the Fondation ARC pour la Recherche Contre le Cancer, the University of Rennes 1 and the Centre National de la Recherche Scientifique. MM and AT are fellows of the Region Bretagne, the Ligue Nationale contre le Cancer and the Fondation ARC pour la Recherche Contre le Cancer. EG is a post-doctoral fellow of the Fondation pour la Recherche Médicale, DEQ20170336742. RG is supported by a Career Development Award, CDA00019/2019-C, from the Human Frontier Science Program. We are grateful to Roger Karess, Valérie Doye and Antoine Guichet (Institut Jacques Monod Paris), Yong Zhang and Shan Jin (Institute of Genetics and Developmental Biology, Beijing), Jorgen Johansen and Hyelee Loyd (Iowa State University), Renata BAsto (Institut Curie, Paris), Mikiko Siomi (University of Tokyo) for the kind gifts of fly stocks, DNA constructs, and antibodies. We would like to thank M. Steinmetz for advices to inactivate the dTBCE CAP-Gly motif, Sébastien Huet, Stéphanie Dutertre and Xavier Pinson for their help using the microscopes of the Microscopy Rennes imaging center facility.

**Author contributions**

Original: Conceptualisation, R. Giet; Methodology, M.M., E.G., R.G., J-P.G and R. Giet; Investigation, M.M., E.G., A.P., C.B., J-P.G, R.G. and R. Giet; Writing – Original Draft: R. Giet; Review & Editing, M.M, E.G., L-R.P., D.C., R.G., L.R-P, C.B. and R.Giet; Funding Acquisition, R.Giet; Resources, R.Giet; Supervision, R.G, D.C., G.G.P., L.R-P. and R. Giet

Revised: Conceptualisation, R. Giet; Methodology, A.T., E.G., and R. Giet, Investigation, A.T., E.G., A.P. and R. Giet; Writing – Revised manuscript, R. Giet; Review & Editing, E.G., R.G., C.B. and R.Giet; Funding Acquisition, R.Giet; Resources, R.Giet ; Supervision, R.Giet.

R.G.: Romain Gibeaux.

**Declaration of interest**

The authors declare no competing interests.

**Figure 1: Dynamic localization of dTBCE variants during mitosis in early embryos**

A) Schematic showing the different dTBCE variants used for live imaging and rescue experiments. The wild-type (WT) dTBCE (top left) harbours an N-terminal CAP-Gly motif, a central leucine-rich region, and a ubiquitin-like domain (UBL) that is predicted to contain a putative weak nuclear localization sequence (NLS) that is not conserved in other members of the family. The dTBCE$^{mutCG}$ variant (where 'mutCG' refers to mutated CAP-Gly) was generated by replacing the most conserved G<u>KH</u>N sequence by G<u>AA</u>N (top right). To mimic the mutation found in human patients with HRD syndrome, we created a dTBCE$^{HRD}$ variant (bottom left) by deleting four amino acids downstream from that GKHN motif. Finally, the putative C-terminal NLS motif (M<u>KR</u>P<u>R</u>L) was mutated into (M<u>AA</u>P<u>A</u>L) to generate a NLS-defective protein, dTBCE$^{mutNLS}$ (bottom right). B-D) Dynamics in dividing embryos of tubulin (Tub) and (B) dTBCE-GFP (Video S1 and Figure S1A); (C) dTBCE$^{mutCG}$-GFP (Video S2 and Figure S1B); (D) dTBCE$^{HRD}$-GFP (Video S3 and Figure S1C); and (E) dTBCE$^{mutNLS}$-GFP (Video S4 and Figure S1D). Note that the mutant dTBCE$^{mutCG}$-GFP (C) lost its association with microtubules and with the nuclear mmbrane, and its ability to be enriched in the nuclear space during prophase. In the merge channel (third column), GFP is green and RFP-α-tubulin is magenta. Scale bar = 10 μm. Times are shown as min:s. See also Figure S2 for the Western blotting analyses of dTBCE-GFP variants.

**Figure 2: Interaction of dTBCE with nuclear pore proteins and components of the Ran pathway.**

Lysates of S2 stable cell lines expressing GFP, dTBCE-GFP, and the non-functional CAP-Gly mutant dTBCE$^{mutCG}$-GFP, were collected and subjected to immunoprecipitation with anti-GFP nanobodies (see Methods). A) To verify the presence of the GFP-tagged proteins, a fraction (5%) of the immunoprecipitation (IP) reaction was analysed by Western blot using an anti-GFP antibody, while the remaining amount was analysed by mass spectrometry. B) Interaction network of proteins that specifically interact with dTBCE but not with GFP or dTBCE$^{mutCG}$-GFP. The cluster was generated by STRING (see Methods). C) List of proteins interacting specifically with dTBCE used for the schema shown in B. D) Anti-GFP Immunoprecipitation experiments were performed from embryo extracts expressing either GFP, dTBCE-GFP or dTBCE$^{mutCG}$-GFP. The inputs (5% of the total extract, *left*) and the immunoprecipitates (IP:GFP, *right*) were analysed by Western blot to confirm the presence of GFP, GFP-tagged dTBCE variants, α-tubulin, Importin α-2 and Ran. E) Gene ontology (GO) classification of dTBCE-interacting proteins absent in GFP or dTBCE$^{mutCG}$-GFP

immunoprecipitates. The graph summarizes the three most significant GO terms for each ontological category. The significance of enrichment is expressed as -log(*p*-value), and the red dashed line indicates a *p*-value threshold of 0.01. The localisation of Ketel-GFP (Importin ß), Venus-Ran, and dTBCD-GFP in early embryos is shown in Figure S3.

**Figure 3: Importance of dTBCE for neural tissue development and mitotic spindle assembly in *Drosophila* neuroblasts**

A) Analysis of dTBCE, α-tubulin, β-tubulin, and actin protein levels in fly neural tissues in control and *dTBCE* RNAi samples. RNAi lines 'KK' and 'GD' (see Methods) were used alone or in combination ('KK+GD') to drive more efficient knockdown of dTBCE. B) *Top,* the two optic lobes and ventral ganglion in a *Drosophila* shown graphically then in control and *dTBCE* (KK+GD) RNAi larval brains. *Bottom,* Dot plot of the mean (± s.d.) brain lobe diameter in control and KK+GD after 2 days of RNAi treatment (control: 172 ± 17 μm, *n* = 14; *dTBCE* RNAi: 161 ± 9 μm, *n* = 14) after 3 and days of RNAi (control: 214 ± 19 μm, *n* = 15, *dTBCE* RNAi: 194 ± 9 μm, *n* = 10). Scale bar = 100 μm. Mann-Whitney test: **, *P* = 0.0011. C) Mitosis in squash preparations stained with DAPI from control or *dTBCE* dsRNA-treated brains. The *dTBCE* RNAi brains show hyper-condensed chromosomes. Fisher test: ****, *P* < 0.00001. Scale bar = 10 μm. D) Histogram showing the mean (± s.d.) mitotic index in control brain tissue (0.73% ± 0.16, 3 brains, *n* = 13,095) and in three *dTBCE* RNAi brain types: KK (2.39% ± 0.35, 4 brains, *n* = 11,535); GD (1.95% ± 0.21, 2 brains, *n* = 6,329); and KK+GD (3.75% ± 0.35, 2 brains, *n* = 6,319). E) Metaphase in control and *dTBCE* RNAi Nbs. In the top row, microtubules (MTs) are red, DNA is green, and lamin is blue. Note the decrease in the mitotic-spindle MT density in *dTBCE* RNAi as compared to the control. F) Mitosis in WT (control) or *dTBCE*-depleted live Nbs expressing Tubulin-GFP (Tub-GFP). Note the lower MT densities (red arrowheads) and the delay between mitotic entry and anaphase onset following dTBCE depletion. Times are shown as min: s. G) Dot plot showing the mean (± s.d.) spindle length in control (12.1 ± 1.5 μm, *n* = 17) and *dTBCE* RNAi Nbs: KK (10.5 ± 1.8 μm, *n* = 17); GD (10.2 ± 1.3 μm, *n* = 14); and combined KK+GD (9.0 ± 1.8 μm, *n* = 25). H) Dot Plot showing mean (± s.d.) mitosis duration in control (5.1 ± 0.6 min, *n* = 67) and *dTBCE* RNAi Nbs: KK (6.1 ± 0.8 min, *n* = 45); GD (6.1 ± 0.8 min, *n* = 17); and KK+GD (7.0 ± 1.0 min, *n* = 32). I) Dot plot showing the mean (± s.d.) Tub-GFP signal intensity in the spindle region in control (0.83 ± 0.13, *n*=15) and *dTBCE* RNAi Nbs: KK (0.44 ± 0.15 min, *n* = 16); GD (0.37 ± 0.09 min, *n* = 13); and KK+GD (0.28 ± 0.09 min, *n* = 15). Mann-Whitney

test: *, $P < 0.05$; **, $P < 0.001$; ***, $P < 0.0001$; ****, $P < 0.00001$. Figure S4 shows the SAC-dependent mitotic delay of dTBCE-knock down dividing cells.

**Figure 4: Contribution of dTBCE to microtubule nucleation around chromatin**

A) Schema of microtubule (MT) depolymerization and regrowth assay a mitotic Nb (see Methods). Fly brains were dissected in Schneider's media and incubated on ice for 30 min to induce total MT depolymerization, then regrowth was induced by a temperature shift to 25 °C. Brains were fixed after 30 s, at which point MT nucleation can be visualized at the centrosomes and around chromatin. A bipolar spindle is formed 90 s after returning to 25 °C. Centrosomes are grey, MTs are red, and DNA is blue. B) Representative images of control and *dTBCE* RNAi mitotic Nbs during MT regrowth after cold-induced MT depolymerization. Samples were analysed immediately after depolymerization, then 30 and 90 s after returning to 25° C. The red arrowhead shows MT nucleation around chromatin at 30 s, which is absent in the *dTBCE* RNAi cells. The bottom row is monochrome, while in the top row the MTs are red, DNA is blue, and γ-tubulin is green. C) Histogram showing the mean (± s.d.) spindle/centrosome ratio of the tubulin signal in control (1.68 ± 0.74, $n = 12$) and dTBCE-depleted Nbs (0.74 ± 0.48, $n = 20$). D) Time-lapse spinning disk confocal microscopy was used to examine control (Video S5) and *dTBCE* RNAi metaphase Nbs (Video S6) expressing EB1-GFP. A single frame is presented in the top row, and the middle row shows 20-time projection (10 s). The bottom row shows kymographs of microtubule plus-end intensity over the time-lapse acquisition (1 min) between the two spindle poles, with a LUT colormap ranging from dark blue to red. Arrows indicate the centrosomal positions. U-track software measurements of the comet velocity in controls (16.75 µm/min, $n = 10$ cells) and *dTBCE* RNAi-treated cells (16.11 µm/min, $n = 12$) were similar ($P = 0.46$, Mann-Whitney test). E) Histogram showing the mean (± s.d.) EB1-GFP fluorescence intensity ratio (a.u.) between chromatin and the centrosome in control (0.84 ± 0.16, $n = 7$) and *dTBCE* RNAi metaphase Nbs (0.46 ± 0.14, $n = 14$). F) Western blot analysis showing the levels of dTBCE, EB1-GFP, and actin in control or dTBCE-depleted brains. Scale bars = 10 µm. Mann-Whitney test *P*-values: ***, $P < 0.001$.

**Figure 5: During prophase, dTBCE mediates tubulin enrichment in the nuclear space**

A) Schema of tubulin enrichment in the nuclear space in the presence (top) or absence (bottom, '+ colchicine') of microtubules (MTs). Depolymerising conditions were used to get rid of tubulin signals from MTs and thus allow an accurate quantification of the signals in the

nucleus. B) Selected live imaging time points of control, *dTBCE,* and Ran-knockdown Nbs expressing mCherry-α-Tubulin during early mitosis after incubation with 20 μM colchicine to depolymerize the MT network. Note the accumulation of tubulin in the nuclear region during mitotic entry in the control (time 00:40). Times are shown as min:s. Scale bar = 10 μm. C) Graphs of the mean (± s.d.) differences in tubulin signal intensity between the nucleus and the cytoplasm over time in control, *dTBCE*-knockdown, and *Ran*-knockdown cells. D) As C, but showing tubulin fluorescence intensity in the nucleus. The corresponding linear regressions are shown in straight bold lines calculated as follows: for control, $y = 0.78x + 0.74$ and $r^2 = 0.97$; for dTBCE knockdown, $y = 0.38x + 0.63$, $r^2 = 0.98$; and for Ran knockdown, $y = 0.22x + 0.23$, $r^2 = 0.98$. The slopes of the curves were calculated in the growing phase, and are significantly different ($P < 0.0001$). E) As D, but this time displaying cytoplasmic tubulin fluorescence intensity. F) Schema of tubulin dynamics in the nucleus during mitosis in control or Nbs depleted for dTBCE or Ran.

**Figure 6: Lamin knockdown accelerates tubulin entry.**

A) Control and *Lam* RNAi fixed Nbs stained for tubulin and lamin. B) Dot plot showing the mean (± s.d.) lamin nuclear fluorescence intensity in control (82.5 ± 26.2, $n = 38$) and *lam* RNAi Nbs (6.2 ± 4.1, $n = 24$). Key: ****, $P < 0.00001$ (Mann-Whitney test). C) Selected images of squash preparations of control and *Lam* RNAi Nbs expressing mCherry-α-tubulin in the presence of colchicine. Time is shown in s. D) Graph of the mean (± s.d.) tubulin fluorescence intensities in the nucleus over time, as well as their corresponding linear regressions (straight bold lines) in control ($n = 19$, $y = 0.49x - 14.6$, $r^2 = 0.98$) and lamin knockdown cells ($n = 15$, $y = 0.72x - 22.1$, $r^2 = 0.98$). The slopes of the curves are significantly different ($P = 0.011$). E) Schema comparing tubulin enrichment in the nuclear space, which occurs more quickly in *Lam* RNAi Nbs than in the controls during early mitosis. Scale bars = 10 μm.

**Figure 7: Dynamic tubulin interactions with dTBCE**

A) GFP, dTBCE-GFP and dTBCE$^{mutCG}$-GFP were immunoprecipitated from S2 cells and bound to GFP-trap beads (green in the merge row). Beads were subsequently incubated with rhodamine-conjugated tubulin (red in the merge) and GTP. The beads were then imaged by spinning disk-confocal microscopy (see Methods). Scale bar = 10 μm. B) Dot plot showing the mean (± s.d.) fluorescence intensities (a.u.) of each sample in the GFP channel calculated

as follows: for GFP, 217.4 ± 56.0, *n* = 42; for TBCE-GFP, 229.9 ± 104.4, *n* = 31; and for $TBCE^{mutCG}$-GFP, 226.2 ± 76.6, *n* = 42). Key: ns, not significant (Mann-Whitney test). C) As B, but showing in the tubulin-rhodamine channel and based on the following values: GFP, 0.4 ± 0.7, *n* = 42; dTBCE-GFP, 25.9 ± 6.2, *n* = 31; and $dTBCE^{mutCG}$-GFP, 4.7 ± 4.0, *n* = 42. Tubulin-rhodamine is present at the surface of the dTBCE-GFP beads, but absent from the GFP beads, and strongly reduced when the dTBCE CAP-Gly motif was mutated. Key: ***, $P < 0.0001$ (Mann-Whitney test). D) Fluorescence recovery after photobleaching (FRAP) in a small region (dotted rectangle) at the surface of dTBCE-GFP beads incubated with tubulin-rhodamine. A recovery of tubulin fluorescence is observed, indicating that there is an exchange between the tubulin that interacts with dTBCE and the tubulin in the free pool. E) Quantification of the TBCE-GFP (*n* = 4) and tubulin-rhodamine (*n* = 9) mean (± s.d.) intensities in the photobleached regions. F) Proposed model for dTBCE-dependent tubulin enrichment in the nuclear space during early mitosis. The red lines are microtubules (MTs), and the intensity of tubulin levels is shaded in red. In wild-type *Drosophila* neural stem cells, dTBCE and nuclear pore components are incorporated first into the nuclear space to create a milieu that can dynamically bind to tubulin (see also Figure S5). Tubulin entry and or enrichment is then facilitated through the dTBCE-CAP-Gly motif in the future spindle region to promote nucleation of MTs around chromosomes. When dTBCE is knocked down, tubulin fails to be efficiently recruited in the nuclear space, and the ensuring low concentrations prevent sufficient MT nucleation around chromatin and thus mitotic spindle assembly is impaired.

## RESOURCE AVAILABILITY

### Lead contact and materials availability

Further information and requests for plasmids, *Drosophila* lines and the dTBCE antibody generated in this study, should be directed and will be fulfilled by the Lead Contact, Régis Giet (regis.giet@univ-rennes1.fr).

### Data and Code Availability

This study did not generate unique code. The Mass Spectrometry dataset generated is available upon request.

## EXPERIMENTAL MODEL AND SUBJECT DETAILS

### Drosophila maintenance

Flies were maintained under standard conditions at 25°C. RNAi against dTBCE and lamin required a temperature shift to 29°C for 48 and 96 hours respectively. Embryos were collected up to 2 hours after egg laying and brains were obtained by dissection of third instar larvae. A list of all the lines used in this study is detailed in the Key Resources Table.

### S2 cells culture

S2R+ cells were cultured at 25°C in Schneider's Drosophila medium supplemented with 10% FCS, penicillin (100 U/mL) and streptamycin (100 U/mL).

## METHOD DETAILS

### DNA constructs

dTBCE open reading frame was amplified by PCR using the GM13256 cDNA gold clone obtained from the Drosophila Genomic Resource Center (DGRC, Indiana University) and cloned without the stop codon into pENTR (Invitrogen) to generate the pENTR-dTBCE entry clone. This clone was subsequently used for mutagenesis using the QuickChange lightning multi site-directed mutagenesis kit (Agilent). The putative weak NLS motif GLVMKRFRLS located in the conserved Ubiquitin-like C-terminal domain of dTBCE was mutated into GLVMAAFALS to generate pENTR-dTBCE$^{mutNLS}$. The HsTBCE deletion nearby the CAP-

Gly domain, observed in patients exhibiting hypoparathyroidism, mental retardation and facial dysmorphism (HRD) was recapitulated by deleting the corresponding IVDG aminoacids sequence of dTBCE to generate pENTR-dTBCE$^{HRD}$ [21]. The conserved CAP-Gly GLRGKHNG motif present in the N-terminal region of dTBCE sequence was mutated into GLRGAANG (Michel Steinmetz, personal communication) to generate pENTR-dTBCE$^{mutCG}$. To generate C-terminal GFP fusion of wild type and mutant dTBCE proteins, the corresponding mutated entry clones were recombined using a LR clonase kit (Invitrogen) into pUWG (for dTBCE and dTBCE$^{HRD}$), pTWV (for dTBCE, dTBCE$^{HRD}$, dTBCE$^{mutCG}$ and dTBCE$^{mutNLS}$), or pPWG (dTBCE, dTBCE$^{HRD}$, dTBCE$^{mutCG}$ and dTBCE$^{mutNLS}$) obtained from the DGRC. dTBCD ORF was amplified by PCR, cloned into pENTR without the STOP codon and recombined into pUWG to generate a dTBCD-GFP *Drosophila* expression construct. The destination vectors were subsequently injected into *Drosophila* embryos for P-element mediated transformation (BestGene). Note that the pUWG destination vector allowed the expression of wild type dTBCE and dTBCD under the control of the poly-ubiquitin promoter, while pPWG and pTWV were used for overexpression with the Gal4/UAS system.
The N-terminal domain of dTBCE (amino acid 1 to 150) was cloned using the Gibson assembly system (New England Biolabs) into pET-23b (Novagen) to generate the pET-23b-Nt-dTBCE vector for expression in *E. coli* and antibody production in guinea pig.
For generation of S2 stable cell lines expressing dTBCE-GFP or dTBCE$^{mutCG}$-GFP, the corresponding entry clones were recombined into Puro-pAWG, allowing expression of C-terminal GFP fusion proteins expressed under the control of the Actin5C promoter, and selection by puromycin (kind gift of Roger Karess, Institut Jaques Monod, Paris).

**Fly stocks**

The *dtbce* mutants flies *tbce$^{LH15}$* and *tbce$^{Z0241}$* have been described previously and correspond to null alleles with embryonic lethality [31]. The *tbce$^{LH15}$/tbce$^{Z0241}$* heteroallelic combination was used in this paper and referred as *dtbce* to assay for rescue by the GFP-tagged dTBCE variants.
Expression of dTBCE-GFP and dTBCE$^{HRD}$-GFP under the control of a polyubiquitin promoter was able to restore full viability of the *dtbce* mutant. Transgenic flies with the following genotypes were used for RNAi or protein expression: TubGal80$^{ts}$; 69B-Gal4 UAS-GFP-α-tubulin, Insc-Gal4, UAS-Cherry-α-tubulin, Actin5C-Gal4 and V32-Gal4 and were obtained from the Bloomington Drosophila Stock Center (Indiana University) and used to drive transgenic constructs or dsRNAs. UASt or UASp mediated expression of dTBCE-GFP,

dTBCE$^{mutCG}$-GFP, dTBCE$^{mutNLS}$-GFP or dTBCE$^{HRD}$-GFP was driven by 69B-Gal4, Actin5C-Gal4 or V32-Gal4.

Transgenic flies carrying UAS and hairpin sequences to knock-down dTBCE (KK105246 and GD34388), Mad2 (KK106003), Ran (GD24835), and Lamin (KK107419), were obtained from the VDRC (Line) Vienna *Drosophila* RNAi Center [45]. Flies expressing the full-length EB1-GFP, Venus-Ran and Ketel-GFP and RFP-α-tubulin were described in previous studies [17, 22, 23, 43, 44].

**Expression and purification of recombinant protein**

The pET-23b-Nt-dTBCE expression vector was transformed into the *E. coli* BL21(DE3) strain (New England Biolabs). The recombinant protein expression was induced with 1mM IPTG during 4 h at 25°C and the bacterial pellet was stored at -20°C until use. The pellet was resuspended on ice, in Lysis Buffer (LB: Tris 10 mM, 10 % Glycerol, 500 mM NaCl, pH7.4) containing 1% Triton X-100 (Sigma), proteases inhibitor tablets (Roche) and lysozyme (1mg/ml). The resuspended bacterial pellet was then sonicated 10 times for 10 s on ice and centrifuged at 10 000 *g* for 30 min at 4°C. The 6xHistidine-tagged Nt-dTBCE protein in the supernatant was purified following the manufacturer's instructions on a Nickel column (Qiagen), dialyzed overnight in PBS at 4°C and used for guinea pig immunization (Covalab).

**Antibodies**

Polyclonal rabbit anti-Ran antibody (ref. ab11693) was from Abcam and used 1:2000 for Western blotting. The YL1/2 rat monoclonal anti-tyrosinated tubulin antibody (ref. Mab1864, 1:200) and the mouse monoclonal and rabbit polyclonal anti-phosphorylated histone H3 (Ser10) antibodies (ref. 06570, 1:1000) were obtained from Millipore. The anti-GFP mouse monoclonal antibody mix (ref. 11814460001, 1:1000) was obtained from Roche. The rabbit C-20 anti-PKCζ (sc-216, 1:200), the mouse anti-β tubulin antibody (ref. sc-365791, 1:1000) and rabbit anti-actin (ref. sc-1616-R, 1:5000) polyclonal antibodies were obtained from Santa Cruz. Mouse anti-Lamin (ref. ADL84.12, 1:200) was from purchased from the Developmental Studies Hybridoma Bank (Iowa University). The mouse monoclonal anti α2-Importin was described before and used at 1:100 for Western blotting [42]. The mouse monoclonal GTU88 anti γ-tubulin was from Sigma and used at 1:500 (ref. T5326). The mouse monoclonal anti-dTBCE antibody was described before [31]. The guinea pig polyclonal anti-Nt-dTBCE (Amino acids 1-150) was used at 1:1000 for immunostaining and at 1:10000 for Western blotting. The mouse DM1α monoclonal anti-α-tubulin antibody was from Sigma (ref.

T6199, 1:2000). Goat secondary peroxidase-conjugated antibodies (1:5000) were obtained from Jackson ImmunoResearch Laboratories, and donkey Alexa Fluor–conjugated secondary antibodies (1:1000) were obtained from Life Technologies.

**Western Blotting analyses**

After transfer of the proteins on a nitrocellulose membrane (GE Healthcare) using a Trans Blot Turbo system (Biorad), the membranes were briefly stained with ponceau S, to ensure sample quality and blocked for 2 h with TBST (20 mM Tris, 150 mM NaCl and 0.1 % Tween20, pH 7.4) containing 10 % skimmed milk (5% and 1% BSA for the anti-Ran and anti-Lamin antibodies respectively). Primary antibody incubation was performed overnight at 4°C in TBST containing 5 % skimmed milk (or 2.5% BSA for the anti-Ran antibody). Incubation with the secondary antibodies was performed in 5 % skimmed milk for 2 h at room temperature. Three 15 min washes in TBST were performed after antibody incubation. For western blotting, ECL reagent (ref. 34095) was purchased from Thermo Fisher Scientific.

**Immunofluorescence**

Immunostaining of brain Nbs was performed as described previously [17]. Briefly, third instar larvae were dissected in TB (Testis Buffer: 183 mM KCl, 47 mM NaCl, 10 mM Tris, and 1 mM EDTA, pH 6.8 MT) and fixed at 25°C for 20 minutes in TB supplemented with 10% formaldehyde and 0.01 % Triton. Brains were washed in PBST (0.1% Triton in PBS) and blocked in PBSTB (1% BSA in PBST). Primary antibodies were incubated overnight at 4°C. After washes, brains were incubated with secondary antibodies 1 hour at room temperature. After washes, samples were mounted in ProLong Gold antifade (ThermoFisher).

For Mts growth recovery after cold treatment, brains were dissected and incubated on ice for 30 minutes in TB. Brains were fixed immediately or after incubation at 25°C for 30 or 90 seconds.

Image acquisition was performed with a SP5 confocal microscope (Leica).

**Live microscopy**

Fresh 0-2 h embryos expressing fluorescent proteins were immobilized on double-sided tape and gently dechorionated by hand with fine point forceps. 8 to 12 embryos were then deposited at the top a drop of halocarbon 700 oil (Sigma) on a glass slide separated by two 22x22 mm coverslips to create a spacer. The embryos were then covered by a 40x22 mm coverslip right before imaging.

Brains expressing the various fluorescent proteins were dissected in Schneider's *Drosophila* medium containing 10% FCS, following a protocol described before [17]. To monitor tubulin import in the nuclear space, the MT network was depolymerized by 10 min incubation in 20 µM colchicine or 30 µM nocodazole (Sigma). The preparations were then sealed with mineral oil (ref. M8410, Sigma). Alternatively, brains were dissected in PBS and loaded on a glass slide. The tissue was then gently flattened in 10 µl of PBS with a 22x22 mm coverslip, the excess of buffer was removed and the preparation was sealed by halocarbon 700 oil to avoid evaporation. The Nbs at the border of the tissue were identified by light microscopy and immediately imaged within 15 min. For bead fluorescence analyses, GFP, dTBCE-GFP and dTBCE$^{mutCG}$-GFP beads were incubated in a 20 µM solution of bovine brain tubulin (PurSolutions, ref: 142001) supplemented with 25 % of tubulin-rhodamine (Tebu) and 1 mM GTP in BRB80 (80mM PIPES, 1mM EGTA, 1mM $MgCl_2$, pH 6.8 with KOH).

Live images were acquired with a CSU-1X spinning-disk system mounted on an inverted microscope (Elipse Ti; Nikon) equipped with an ILAS2 FRAP head and a 60X 1.4 NA objective at 25°C. Z series were acquired every 1, 30 or 60 s with a CCD camera (CoolSnap HQ2; Photometrics) and a sCMOS ORCA Flash 4.0 (Hamamatsu) controlled by MetaMorph acquisition software version X.

**Immunoprecipitation**

Stable S2 cells expressing GFP, dTBCE-GFP and dTBCE$^{mutCG}$-GFP were grown and collected by centrifugation at 500 *g* for 2 min. The cells were gently resuspended in PBS at 500 *g* for 2 min, the cell pellets were flash frozen in liquid nitrogen and stored at -80°C or processed immediately for immunoprecipitation. A cell pellet, corresponding to $10^8$ cells was resuspended in 0.5 ml of lysis buffer containing 10 mM Tris, 150 mM NaCl, 0.5 mM EDTA, protease and phosphatase inhibitors (Roche). The resuspended cell pellet was sonicated 10 times for 10 s on ice and centrifuged at 10 000 *g* for 30 min at 4°C. The supernatant was then incubated with 10 µl of a GFP-TRAP-MA beads that were previously washed with lysis buffer (Chromotek). Immunoprecipitation was performed for 1 h at 4°C. The beads were then subjected to 3 washes for 5 min each, transferred in a new tube and analysed by Western blotting or subjected to mass spectrometry (see below). For tubulin *in vitro* binding assays, we collected *Drosophila* embryos from females expressing GFP, dTBCE-GFP and dTBCE$^{mutCG}$-GFP proteins. Four hours collections were used, corresponding to early dividing embryos. The embryos were washed with deionized water and immediately flash frozen in liquid

nitrogen and stored at -80°C before use for immunoprecipitation. Lysis and immunoprecipitation were performed similarly to S2 cell pellets except that 250 µl of embryos was used for each immunoprecipitation to saturate the beads with an excess of GFP-tagged proteins.

**On-beads protein digestion**

Beads were resuspended in a digestion buffer containing 75 mM ammonium bicarbonate, pH 8.0, reduced using 10 mM DTT for 20 min and then alkylated at room temperature for 20 min in the dark with 40 mM chloroacetamide. Proteins bound to beads were digested with 1 µg of Trypsin/Lys-C mix (Promega) for 3 h at 37 °C and then supplemented with and additional amount of 150 ng Trypsin/Lys-C for overnight digestion on an end-over-end rotation apparatus at 37 °C. Peptides were isolated on C18 tips according to the manufacturer's instructions (Thermo Fisher Scientific) and dried to completion in a SpeedVac concentrator equipped with an integrated -100°C condensation trap.

**LC-MS/MS analysis**

Peptide samples were analysed by nano LC-MS/MS on a Dionex UltiMate 3000 nanoRSLC chromatography system (Thermo Fisher Scientific / Dionex Softron GmbH, Germering, Germany) connected to an Orbitrap Fusion™ Tribrid™ mass spectrometer (Thermo Fisher Scientific, San Jose, CA, USA) equipped with a nanoelectrospray ion source. Peptides were trapped at 20 µl/min in loading solvent (2% acetonitrile, 0.05% TFA) on a 5mm x 300 µm C18 pepmap cartridge pre-column (Thermo Fisher Scientific / Dionex Softron GmbH, Germering, Germany) during 5 min. Then, the pre-column was switched online with Pepmap Acclaim column (Thermo Fisher Scientific) 50 cm x 75µm internal diameter separation column and the peptides were eluted with a linear gradient from 5-40% solvent B (A: 0.1% formic acid, B: 80% acetonitrile, 0.1% formic acid) in 30 min, at 300 nl/min. Mass spectra were acquired using a data dependent acquisition mode using Thermo XCalibur software version 4.1.50. Full scan mass spectra (350 to 1800 *m/z*) were acquired in the Orbitrap using an AGC target of 4e5, a maximum injection time of 50 ms and a resolution of 120 000. Internal calibration using lock mass on the *m/z* 445. 12003 siloxane ion was used. Each MS scan was followed by acquisition of fragmentation MS/MS spectra of the most intense ions for a total cycle time of 3 s (top speed mode). The selected ions were isolated using the quadrupole analyser in a window of 1.6 *m/z* and fragmented by Higher energy Collision-induced Dissociation (HCD) with 35% of collision energy. The resulting fragments were

detected by the linear ion trap in rapid scan rate with an AGC target of 1e4 and a maximum injection time of 50ms. Dynamic exclusion of previously fragmented peptides was set for a period of 20 s and a tolerance of 10 ppm.

## QUANTIFICATION AND STATISTICAL ANALYSIS

### Statistical Analysis

All statistical tests and data analyses were performed using the Prism7 software (Graphpad). The statistical tests used, the exact value of n and what it represents, the mean, the standard deviation (s.d.), the significance (range or exact *P* values) and the regression line equations (for Figures 5 and 6) are indicated in Figure legends. The Wilcoxon-Mann-Whitney test was used to compare the means of independent samples with non-normal distribution. A two-sided Fisher's exact test was used to assess differences between proportions (mitotic indices). Comparisons of slopes for tubulin entry in the nuclear space were assessed using the linear regression tool. Significance was defined as followed: ns, $P > 0.05$; *, $P < 0.05$; **, $P < 0.001$; ***, $P < 0.0001$; ****, $P < 0.00001$. Samples were not randomized. For most experiments, at least 10 cells, beads or brain lobes were analyzed per condition or genotype.

### dTBCE variants functionality analysis

To analyze the functionality of UAS mediated expression of dTBCE-GFP, dTBCE$^{HRD}$-GFP, dTBCE$^{mutCG}$-GFP and dTBCE$^{mutNLS}$-GFP, twenty *dtbce*$^{Z0241}$; Act5c-GAL4/ T(2-3) females were crossed with ten males *dtbce*$^{LH15}$/Cyo flies carrying the transgene to be tested (insertion on the third chromosome and balanced by TM6b). The ability to fully rescue the *dtbce* mutant was determined by counting the percentage of adult flies lacking the *Cyo* and *Tubby* marker in the progeny. The transgenic dTBCE variants were considered as fully functional when at least one transgenic insertion (three different transgenes were tested) was able to fully restore fly viability, leading to the presence of 33 % of flies without Cyo wings in the progeny ($n$>100 flies). The mutations of the CAP-Gly motif and of the weak putative NLS located in the Ubiquitin-Like domain failed to rescue the *dtbce* mutation.

### Mitotic Timing analysis

Mitotic timing was calculated as described before in *Drosophila* fly brain Nbs [17, 46-48]. Briefly, the mitotic entry point was determined when an increase of GFP or mCherry-tagged tubulin signal was detected in the nuclear region, reflecting dismantlement and permeabilization of

the nuclear envelope to tubulin. Anaphase onset was determined as the first spindle elongation time point.

**Mts polymerization speed**

Analysis of EB1-GFP comet velocity was performed with the U-track software as described before [50].

**LC-MS/MS dataset analyses**

*Database search*

Mass spectra data generated by the Orbitrap™ Fusion™ Tribrid™ instrument (*.raw files) were analysed by MaxQuant [51] (version 1.5.2.8) using default settings and label-free quantification (LFQ). Andromeda [52] was used to search the MS/MS data against a FASTA-formatted *Drosophila melanogaster* reference proteome downloaded from Uniprot [53] (21 923 entries) and complemented with a list of common contaminants (245 entries) maintained by MaxQuant and concatenated with the reversed version of all sequences (decoy mode). The minimum peptide length was set to 7 amino acids and trypsin was specified as the protease allowing up to two missed cleavages. Carbamidomethylation of cysteines [+57.02146 Da] was set as a fixed modification while the following mass additions were used as variable modifications: oxidation of methionine [+15.99491 Da], deamidation of asparagine and glutamine [+0.98401 Da], N-terminal and lysine acetylation [+42.01056 Da] and and pyro-glu from glutamic acid[-18.01055 Da] and glutamine [-17.02654 Da]. The reverse (decoy) and common contaminant hits were removed from the final output.

*Functional annotation*

The Database for Annotation, Visualization and Integrated Discovery (DAVID) [54, 55] was used for protein annotation. The functional annotation tool was used to perform Gene Ontology (GO) classifications of the corresponding genes using the default settings (http://david.abcc.ncifcrf.gov/). TBCE-interacting proteins whose interaction is lost upon alanine substitution of critical amino acids in the CAP-GLY domain were selected for GO analysis. The three most significant GO categories terms for each sub-ontologies (based on GO terms *p-values*) were selected.

*Protein network modelling*

Protein–protein interaction (PPI) network of TBCE was constructed using the STRING database (https://string-db.org/) [56]. A cluster of proteins with GO assignments in the following terms were selected to generate a specific sub-network of TBCE-interacting proteins: *Biological process*: protein import into nucleus; *Cellular component*: nuclear pore; *Molecular function*: structural constituent of nuclear pore.

**KEY RESOURCES TABLE**

| REAGENT or RESOURCE | SOURCE | IDENTIFIER |
|---|---|---|
| **Antibodies** | | |
| Mouse DM1A monoclonal anti-α-tubulin | Sigma | T6199 |
| Mouse polyclonal anti-β-tubulin (E-10) | Santa Cruz | sc-365791 |
| Rabbit polyclonal anti-PKCζ (C-20) | Santa Cruz | sc-216 |
| Rabbit polyclonal anti-phosphorylated histone H3 (Ser10) | Millipore | 06-570 |
| Mouse monoclonal anti-phosphorylated histone H3 (Ser10) clone CMA312 | Millipore | 05-1336 |
| Rat YL1/2 monoclonal anti tyrosinated tubulin | Millipore | MAB1864 |
| Mouse monoclonal anti-dTBCE | [31] | |
| Guinea Pig polyclonal anti-Nt-dTBCE (aa 1-207) | This study | |
| Mouse monoclonal anti-GFP | Roche (Sigma) | 11814460001 |
| Rabbit polyclonal anti-Ran | Abcam | ab11693 |
| Mouse anti-lamin | Developmental Studies Hybridoma Bank | ADL84.12 |
| Mouse monoclonal anti-Imp-α2 | [42] | |
| Rabbit polyclonal anti-Actin (I-19) | Santa Cruz | sc-1616-R |
| Mouse monoclonal anti-γ-tub GTU-88 | Sigma | T5326 |
| **Biological Samples** | | |
| Brain samples | | |
| Early embryos | | |
| S2R+ cells | | |
| **Chemicals, Peptides, and Recombinant Proteins** | | |
| Colchicine | Sigma | C3915 |
| **Experimental Models: Cell Lines** | | |
| Drosophila S2R+ cells | Drosophila Genomics Resource Center (DGRC) | 150 |
| Drosophila S2R+ cells expressing GFP | This study | |
| Drosophila S2R+ cells expressing dTBCE-GFP | This study | |
| Drosophila S2R+ cells expressing dTBCE$^{mutCG}$-GFP | This study | |
| **Experimental Models: Drosophila melanogaster** | | |
| *w* ; *dtbce$^{LH15}$* / CyO ; | [31] | |
| *w* ; *dtbce$^{Z0241}$* / CyO ; | [31] | |
| *w* ; ; UASp-dTBCE-GFP | This study | |
| *w* ; ; UASp-dTBCE$^{mutNLS}$-GFP | This study | |

| | | |
|---|---|---|
| *w* ; ; UASp-dTBCE$^{mutCG}$-GFP | This study | |
| *w* ; ; UASp-dTBCE$^{HRD}$-GFP | This study | |
| *w* ; ; Ubi-dTBCE-GFP | This study | |
| *w* ; ; Ubi-dTBCE$^{HRD}$-GFP | This study | |
| *w* ; ; UAS-GFP-α-tub84B / TM3 | Bloomington Drosophila Stock Center (BDSC) | 7373 |
| *w* ; Ubi-RFP-α-tubulin | [43] | |
| *w* ; ; dTBCE GD10779 / TM3 | Vienna Drosophila Resource Center (VDRC) | 34388 |
| *w* ; dTBCE KK100119 | VDRC | 105246 |
| *w* ; Mad2 KK108038 | VDRC | 106003 |
| *w* ; Ran GD8203 | VDRC | 24835 |
| *w* ; Lamin KK102399 | VDRC | 107419 |
| *w* ; ; UASp-Venus-Ran | [22] | |
| *w* ; Ketel-GFP trapline | [23, 44] | |
| *w* ; ; Ubi-EB1-GFP | [17] | |
| *w* ; Actin5C-Gal4 / CyO | BDSC | 4414 |
| *w* ; V32-Gal4 | BDSC | 7062 |
| *w* ; Inscuteable-Gal4 ; UAS-mCherry Tub | BDSC | 25773 |
| *w* ; Tub-Gal80$^{ts}$ ; TM2 / TM6b | BDSC | 7019 |
| *w* ; ; 69B-Gal4 | BDSC | 1774 |
| *w* ; ; UASt-dTBCE-Venus | This study | |
| *w* ; ; UASt-dTBCE$^{mutNLS}$-Venus | This study | |
| *w* ; ; UASt-dTBCE$^{mutCG}$-Venus | This study | |
| *w* ; ; UASt-dTBCE$^{HRD}$-Venus | This study | |
| *w, y,* Ubi-GFP ; ; | BDSC | 1681 |
| **Oligonucleotides** | | |
| To clone pENTR-dTBCD | | |
| Fwd: **CACC**gccATGTCGAATTCTGTGG | This study | |
| Rev: TTTATCAGCACTCGCTTGCTGC | This study | |
| To clone pENTR-dTBCE | | |
| Fwd: **CACC**gcgATGGTGGGAATTATCG | This study | |
| Rev: TTGAACCAAAACTGTATCATGC | This study | |
| To generate dTBCE$^{mutCG}$ and dTBCE$^{mutNLS}$ mutants from pENTR-dTBCE (QuickChange lightning multi site-directed mutagenesis kit) | | |
| mutCG: GGACTGCGTGGCGCAGCCAACGGCATCGTG | This study | |
| mutNLS: GGATTGGTTATGGCGGCATTCGCGTTAAGCGGT | This study | |
| To generate dTBCE$^{HRD}$ mutant from pENTR-dTBCE (Gibson Assembly) | | |
| Fwd: C**AAGCGCTACTTTCAG**ACGCAGACACCCACG | This study | |
| Rev: **CTGAAAGTAGCGCTTG**CCGTTGTGTTTGCCAC | This study | |
| To clone pET23b-Nt-dTBCE (Gibson Assembly) | | |
| Nt-Fwd: **gatatacat**ATGGTGGGAATTATCGATGAGG | This study | |

| | | |
|---|---|---|
| Nt-Rev: **gctcgagACCGGCAGC**GTTTACCGGCGTCTGGTC | This study | |
| pET-23b-Fwd: **GCTGCCGGTctcgagc**accaccaccaccaccactgagatcc | This study | |
| pET-23b-Rev: **CCACCATatgtatatc**tccttcttaaagttaaacaaaattatttctagagg | This study | |
| **Recombinant DNA** | | |
| pOT2-dTBCE | DGRC | GM13256 |
| pENTR-dTBCE | This study | |
| pENTR-dTBCE$^{mutNLS}$ | This study | |
| pENTR-dTBCE$^{mutCG}$ | This study | |
| pENTR-dTBCE$^{HRD}$ | This study | |
| pUWG | DGRC | 1284 |
| pUbi-dTBCE-GFP | This study | |
| pUbi-dTBCE$^{HRD}$-GFP | This study | |
| pTWV | DGRC | 1092 |
| pUASt-dTBCE-Venus | This study | |
| pUASt-dTBCE$^{mutNLS}$-Venus | This study | |
| pUASt-dTBCE$^{mutCG}$-Venus | This study | |
| pUASt-dTBCE$^{HRD}$-Venus | This study | |
| pPWG | DGRC | 1078 |
| pUASp-dTBCE-GFP | This study | |
| pUASp-dTBCE$^{mutNLS}$-GFP | This study | |
| pUASp-dTBCE$^{mutCG}$-GFP | This study | |
| pUASp-dTBCE$^{HRD}$-GFP | This study | |
| pET-23b | Novagen (Merck) | 69746 |
| pET-23b-Nt-dTBCE | This study | |
| Puro-pAWG | Gift from R. Karess | |
| Puro-pActin5C-dTBCE-GFP | This study | |
| Puro-pActin5C-dTBCE$^{mutCG}$-GFP | This study | |
| pBS-SK(-)-dTBCD | DGRC | LD16031 |
| pUbi-dTBCD-GFP | This study | |
| **Software and Algorithms** | | |
| Fiji | fiji.sc | |
| Prism version 7 | GraphPad | |

## References


1. Desai, A. & Mitchison, T.J. Microtubule polymerization dynamics. *Annu Rev Cell Dev Biol* **13**, 83-117 (1997).
2. Kollman, J.M., Merdes, A., Mourey, L. & Agard, D.A. Microtubule nucleation by gamma-tubulin complexes. *Nat Rev Mol Cell Biol* **12**, 709-721 (2011).
3. Roostalu, J. & Surrey, T. Microtubule nucleation: beyond the template. *Nat Rev Mol Cell Biol* **18**, 702-710 (2017).
4. Goshima, G., Mayer, M., Zhang, N., Stuurman, N. & Vale, R.D. Augmin: a protein complex required for centrosome-independent microtubule generation within the spindle. *J Cell Biol* **181**, 421-429 (2008).
5. Petry, S., Groen, A.C., Ishihara, K., Mitchison, T.J. & Vale, R.D. Branching microtubule nucleation in Xenopus egg extracts mediated by augmin and TPX2. *Cell* **152**, 768-777 (2013).
6. Kalab, P. & Heald, R. The RanGTP gradient - a GPS for the mitotic spindle. *J Cell Sci* **121**, 1577-1586 (2008).
7. Dumont, J. *et al.* A centriole- and RanGTP-independent spindle assembly pathway in meiosis I of vertebrate oocytes. *J Cell Biol* **176**, 295-305 (2007).
8. Cesario, J. & McKim, K.S. RanGTP is required for meiotic spindle organization and the initiation of embryonic development in Drosophila. *J Cell Sci* **124**, 3797-3810 (2011).
9. Moutinho-Pereira, S. *et al.* Genes involved in centrosome-independent mitotic spindle assembly in Drosophila S2 cells. *Proc Natl Acad Sci U S A* **110**, 19808-19813 (2013).
10. Maresca, T.J. *et al.* Spindle assembly in the absence of a RanGTP gradient requires localized CPC activity. *Curr Biol* **19**, 1210-1215 (2009).
11. Woodruff, J.B. *et al.* The Centrosome Is a Selective Condensate that Nucleates Microtubules by Concentrating Tubulin. *Cell* **169**, 1066-1077 e1010 (2017).
12. Baumgart, J. *et al.* Soluble tubulin is significantly enriched at mitotic centrosomes. *J Cell Biol* (2019).
13. Hayashi, H., Kimura, K. & Kimura, A. Localized accumulation of tubulin during semi-open mitosis in the Caenorhabditis elegans embryo. *Mol Biol Cell* **23**, 1688-1699 (2012).
14. Schweizer, N., Pawar, N., Weiss, M. & Maiato, H. An organelle-exclusion envelope assists mitosis and underlies distinct molecular crowding in the spindle region. *J Cell Biol* **210**, 695-704 (2015).
15. Yao, C. *et al.* A nuclear-derived proteinaceous matrix embeds the microtubule spindle apparatus during mitosis. *Mol Biol Cell* **23**, 3532-3541 (2012).
16. Tian, G. & Cowan, N.J. Tubulin-specific chaperones: components of a molecular machine that assembles the alpha/beta heterodimer. *Methods Cell Biol* **115**, 155-171 (2013).
17. Gallaud, E. *et al.* Ensconsin/Map7 promotes microtubule growth and centrosome separation in Drosophila neural stem cells. *J Cell Biol* **204**, 1111-1121 (2014).
18. Hughes, J.R. *et al.* A microtubule interactome: complexes with roles in cell cycle and mitosis. *PLoS Biol* **6**, e98 (2008).
19. Akhmanova, A. & Steinmetz, M.O. Microtubule +TIPs at a glance. *J Cell Sci* **123**, 3415-3419 (2012).
20. Steinmetz, M.O. & Akhmanova, A. Capturing protein tails by CAP-Gly domains. *Trends Biochem Sci* **33**, 535-545 (2008).

21. Parvari, R. *et al.* Mutation of TBCE causes hypoparathyroidism-retardation-dysmorphism and autosomal recessive Kenny-Caffey syndrome. *Nat Genet* **32**, 448-452 (2002).
22. Yao, C. *et al.* Evidence for a role of spindle matrix formation in cell cycle progression by antibody perturbation. *PLoS One* **13**, e0208022 (2018).
23. Villanyi, Z., Debec, A., Timinszky, G., Tirian, L. & Szabad, J. Long persistence of importin-beta explains extended survival of cells and zygotes that lack the encoding gene. *Mechanisms of development* **125**, 196-206 (2008).
24. Okumura, M., Sakuma, C., Miura, M. & Chihara, T. Linking cell surface receptors to microtubules: tubulin folding cofactor D mediates Dscam functions during neuronal morphogenesis. *J Neurosci* **35**, 1979-1990 (2015).
25. Miyake, N. *et al.* Biallelic TBCD Mutations Cause Early-Onset Neurodegenerative Encephalopathy. *American journal of human genetics* **99**, 950-961 (2016).
26. Donaldson, M.M., Tavares, A.A., Ohkura, H., Deak, P. & Glover, D.M. Metaphase arrest with centromere separation in polo mutants of Drosophila. *J Cell Biol* **153**, 663-676 (2001).
27. Tian, G. *et al.* Tubulin subunits exist in an activated conformational state generated and maintained by protein cofactors. *J Cell Biol* **138**, 821-832 (1997).
28. Nithianantham, S. *et al.* Tubulin cofactors and Arl2 are cage-like chaperones that regulate the soluble alphabeta-tubulin pool for microtubule dynamics. *eLife* **4** (2015).
29. Feierbach, B., Nogales, E., Downing, K.H. & Stearns, T. Alf1p, a CLIP-170 domain-containing protein, is functionally and physically associated with alpha-tubulin. *J Cell Biol* **144**, 113-124 (1999).
30. Lopez-Fanarraga, M., Avila, J., Guasch, A., Coll, M. & Zabala, J.C. Review: postchaperonin tubulin folding cofactors and their role in microtubule dynamics. *Journal of structural biology* **135**, 219-229 (2001).
31. Jin, S. *et al.* Drosophila Tubulin-specific chaperone E functions at neuromuscular synapses and is required for microtubule network formation. *Development* **136**, 1571-1581 (2009).
32. Chen, K. *et al.* Arl2- and Msps-dependent microtubule growth governs asymmetric division. *J Cell Biol* **212**, 661-676 (2016).
33. Baffet, A.D. *et al.* Drosophila tubulin-binding cofactor B is required for microtubule network formation and for cell polarity. *Mol Biol Cell* **23**, 3591-3601 (2012).
34. Bhamidipati, A., Lewis, S.A. & Cowan, N.J. ADP ribosylation factor-like protein 2 (Arl2) regulates the interaction of tubulin-folding cofactor D with native tubulin. *J Cell Biol* **149**, 1087-1096 (2000).
35. Fleming, J.A., Vega, L.R. & Solomon, F. Function of tubulin binding proteins in vivo. *Genetics* **156**, 69-80 (2000).
36. Strunov, A. *et al.* Ultrastructural analysis of mitotic Drosophila S2 cells identifies distinctive microtubule and intracellular membrane behaviors. *BMC biology* **16**, 68 (2018).
37. Roubinet, C., White, I.J. & Baum, B. Asymmetric nuclear division of neural stem cells contributes to the formation of sibling nuclei with different identities. *bioXriv* (2020).
38. Tsai, M.Y. *et al.* A mitotic lamin B matrix induced by RanGTP required for spindle assembly. *Science* **311**, 1887-1893 (2006).
39. Silverman-Gavrila, R.V. & Wilde, A. Ran is required before metaphase for spindle assembly and chromosome alignment and after metaphase for chromosome segregation and spindle midbody organization. *Mol Biol Cell* **17**, 2069-2080 (2006).

40. Bellouze, S. *et al.* Golgi fragmentation in pmn mice is due to a defective ARF1/TBCE cross-talk that coordinates COPI vesicle formation and tubulin polymerization. *Hum Mol Genet* **23**, 5961-5975 (2014).
41. Schaefer, M.K. *et al.* Progressive motor neuronopathy: a critical role of the tubulin chaperone TBCE in axonal tubulin routing from the Golgi apparatus. *J Neurosci* **27**, 8779-8789 (2007).
42. Yashiro, R. *et al.* Piwi Nuclear Localization and Its Regulatory Mechanism in Drosophila Ovarian Somatic Cells. *Cell reports* **23**, 3647-3657 (2018).
43. Basto, R. *et al.* Centrosome amplification can initiate tumorigenesis in flies. *Cell* **133**, 1032-1042 (2008).
44. Morin, X., Daneman, R., Zavortink, M. & Chia, W. A protein trap strategy to detect GFP-tagged proteins expressed from their endogenous loci in Drosophila. *Proc Natl Acad Sci U S A* **98**, 15050-15055 (2001).
45. Dietzl, G. *et al.* A genome-wide transgenic RNAi library for conditional gene inactivation in Drosophila. *Nature* **448**, 151-156 (2007).
46. Caous, R. *et al.* Spindle assembly checkpoint inactivation fails to suppress neuroblast tumour formation in aurA mutant Drosophila. *Nat Commun* **6**, 8879 (2015).
47. Metivier, M. *et al.* Dual control of Kinesin-1 recruitment to microtubules by Ensconsin in Drosophila neuroblasts and oocytes. *Development* **146** (2019).
48. Gogendeau, D. *et al.* Aneuploidy causes premature differentiation of neural and intestinal stem cells. *Nat Commun* **6**, 8894 (2015).
49. Rueden, C.T. *et al.* ImageJ2: ImageJ for the next generation of scientific image data. *BMC bioinformatics* **18**, 529 (2017).
50. Jaqaman, K. *et al.* Robust single-particle tracking in live-cell time-lapse sequences. *Nature methods* **5**, 695-702 (2008).
51. Tyanova, S., Temu, T. & Cox, J. The MaxQuant computational platform for mass spectrometry-based shotgun proteomics. *Nature protocols* **11**, 2301-2319 (2016).
52. Cox, J. *et al.* Andromeda: a peptide search engine integrated into the MaxQuant environment. *Journal of proteome research* **10**, 1794-1805 (2011).
53. UniProt, C. UniProt: a worldwide hub of protein knowledge. *Nucleic Acids Res* **47**, D506-D515 (2019).
54. Huang da, W., Sherman, B.T. & Lempicki, R.A. Systematic and integrative analysis of large gene lists using DAVID bioinformatics resources. *Nature protocols* **4**, 44-57 (2009).
55. Huang da, W., Sherman, B.T. & Lempicki, R.A. Bioinformatics enrichment tools: paths toward the comprehensive functional analysis of large gene lists. *Nucleic acids research* **37**, 1-13 (2009).
56. Jensen, L.J. *et al.* STRING 8--a global view on proteins and their functional interactions in 630 organisms. *Nucleic acids research* **37**, D412-416 (2009).

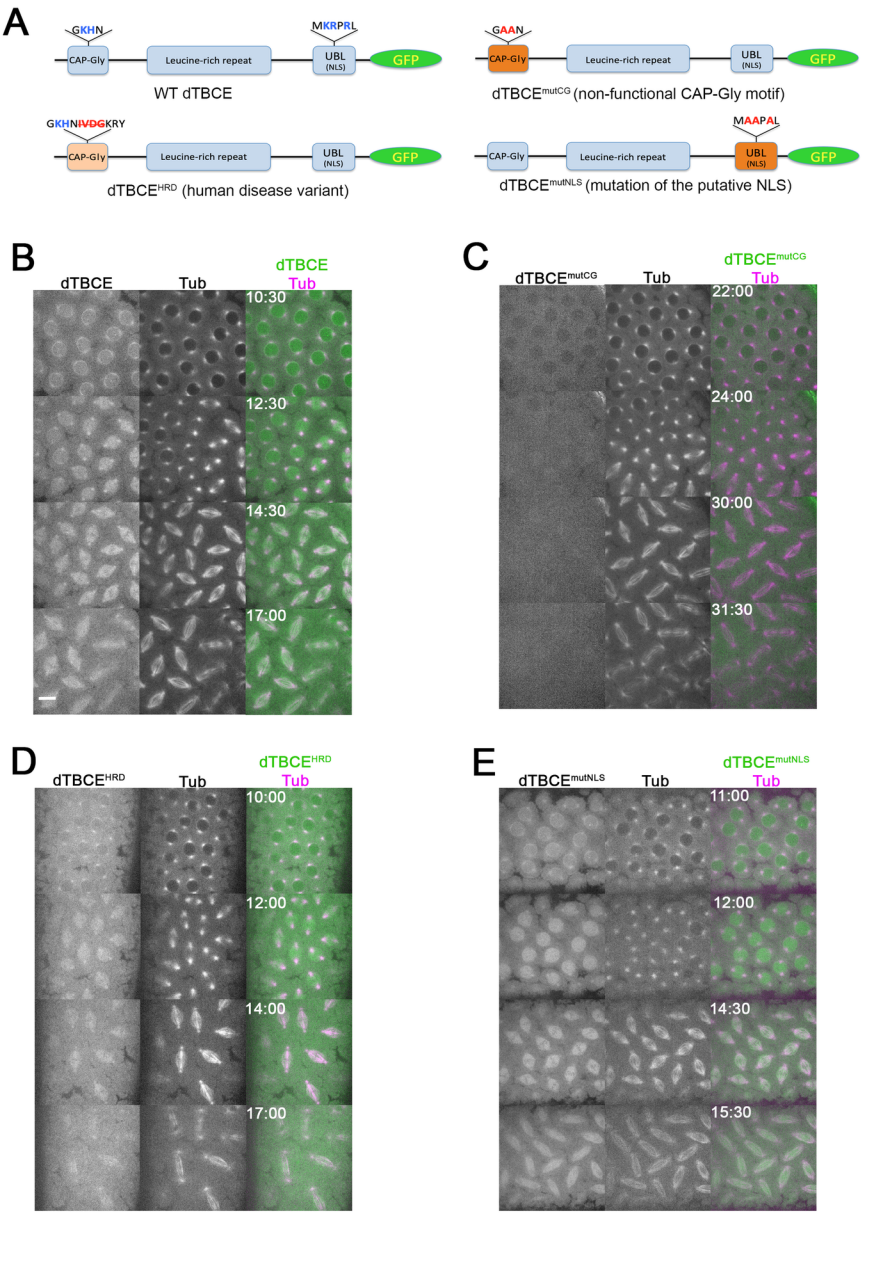
A
GKHN
CAP-Gly
Leucine-rich repeat
MKRPRL
UBL
(NLS)
GFP
WT dTBCE
GAAN
CAP-Gly
Leucine-rich repeat
UBL
(NLS)
GFP
dTBCEmutCG (non-functional CAP-Gly motif)
GKHNIVDGKRY
CAP-Gly
Leucine-rich repeat
UBL
(NLS)
GFP
dTBCEHRD (human disease variant)
MAAPAL
CAP-Gly
Leucine-rich repeat
UBL
(NLS)
GFP
dTBCEmutNLS (mutation of the putative NLS)
B
dTBCE
Tub
dTBCE
Tub
10:30
12:30
14:30
17:00
C
dTBCEmutCG
Tub
dTBCEmutCG
Tub
22:00
24:00
30:00
31:30
D
dTBCEHRD
Tub
dTBCEHRD
Tub
10:00
12:00
14:00
17:00
E
dTBCEmutNLS
Tub
dTBCEmutNLS
Tub
11:00
12:00
14:30
15:30

A

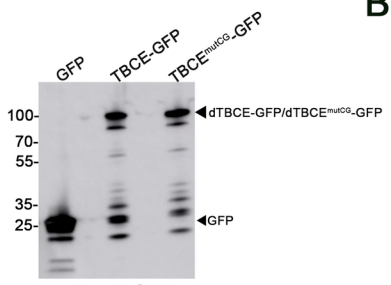


B

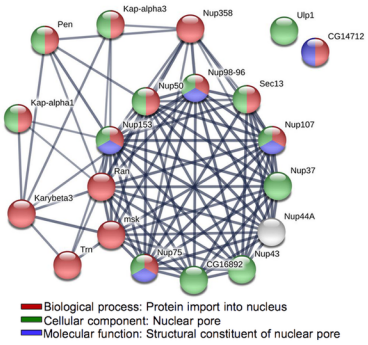


C

| Uniprot accession | Description | Gene name |
|---|---|---|
| Q9W351 | CG16892 / Aladin | CG16892 / Aladin |
| Q9VGL0 | LD43047p | CG14712 |
| O76521 | Importin subunit alpha | Kap-alpha1 |
| Q9V455 | Importin subunit alpha | Kap-alpha3 |
| Q9VN44 | FI07923p | Karybeta3 |
| Q9VSD6 | D-Importin 7/RanBP7 | msk |
| Q9V466 | Nuclear pore complex protein Nup107 | Nup107 |
| Q9VXE6 | Nuclear pore complex protein Nup153 | Nup153 |
| Q9VBU7 | Nucleoporin 358kD | Nup358 |
| Q9VBU8 | Nucleoporin 37kD | Nup37 |
| Q9VE85 | Nucleoporin 43kD | Nup43 |
| Q7K2X8 | Nucleoporin at 44A | Nup44A |
| Q7K0D8 | Nuclear pore complex protein Nup50 | Nup50 |
| A1YK02 | Nuclear pore complex protein Nup75 | Nup75 |
| Q9VCH5 | Nucleoporin 98-96kD | Nup98-96 |
| P52295 | Importin subunit alpha | Pen |
| A4V4A5 | GTP-binding nuclear protein | Ran |
| Q9V3J4 | Protein SEC13 homolog | Sec13 |
| Q9VRV8 | FI21453p1 / Transportin | Trn |
| Q9VWK5 | GH15225p | Ulp1 |

D

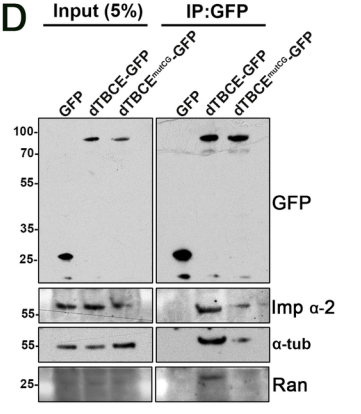


E

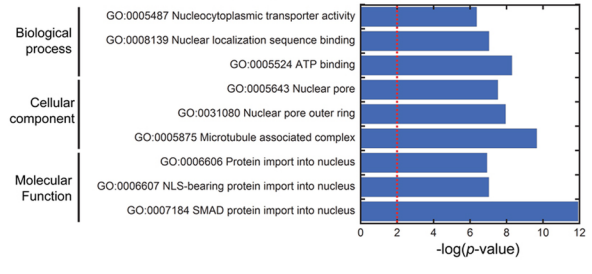

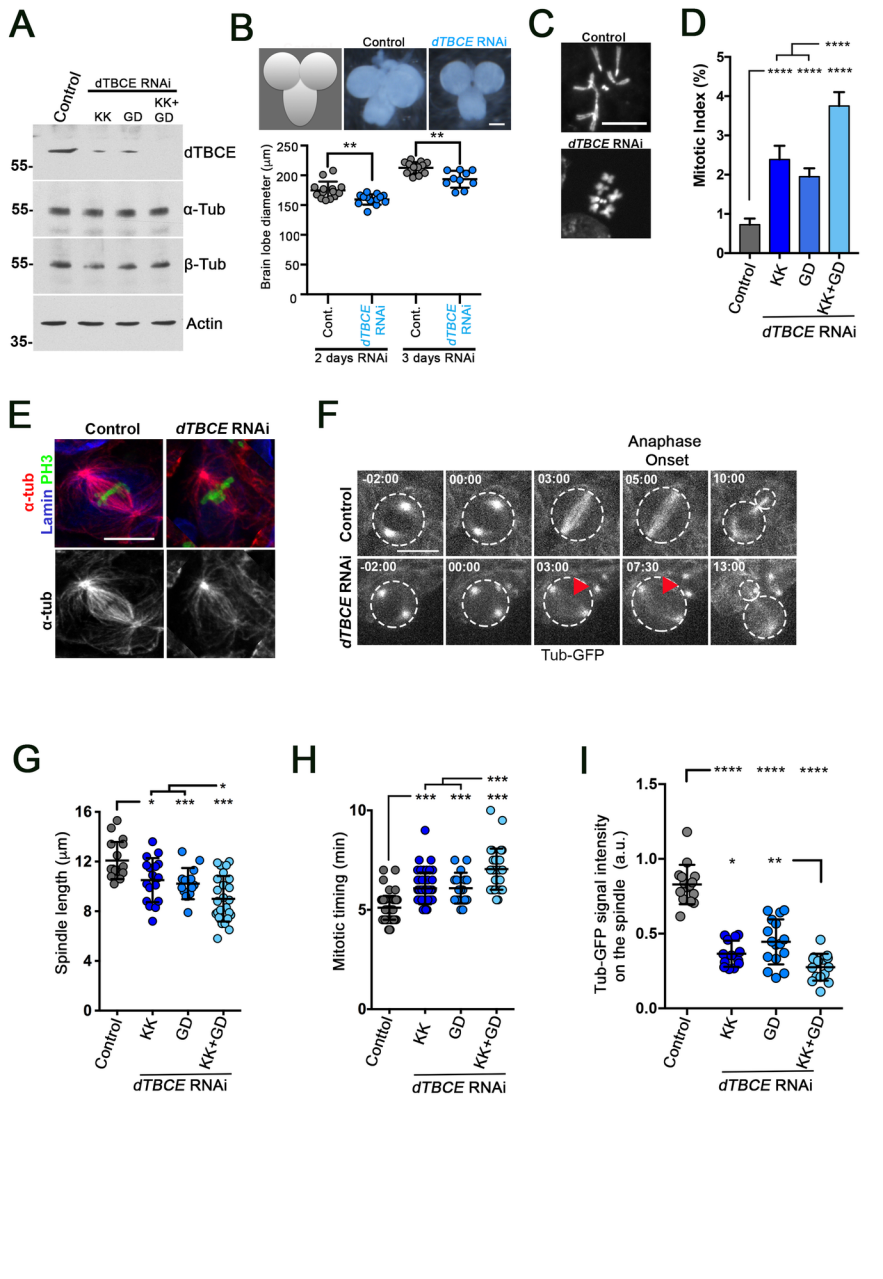
A
Control
dTBCE RNAi
KK
GD
KK+GD
55-
55-
55-
35-
dTBCE
α-Tub
β-Tub
Actin
B
Control
dTBCE RNAi
Brain lobe diameter (μm)
250
200
150
100
50
0
**
**
Cont.
dTBCE RNAi
Cont.
dTBCE RNAi
2 days RNAi
3 days RNAi
C
Control
dTBCE RNAi
D
Mitotic Index (%)
5
4
3
2
1
0
****
****
****
****
Control
Kk
GD
Kk+GD
dTBCE RNAi
E
Control
dTBCE RNAi
α-tub
Lamin PH3
α-tub
F
Anaphase Onset
Control
dTBCE RNAi
-02:00
00:00
03:00
05:00
10:00
-02:00
00:00
03:00
07:30
13:00
Tub-GFP
G
Spindle length (μm)
16
12
8
4
0
*
***
*
***
Control
Kk
GD
Kk+GD
dTBCE RNAi
H
Mitotic timing (min)
10
5
0
***
***
***
Control
Kk
GD
Kk+GD
dTBCE RNAi
I
Tub-GFP signal intensity on the spindle (a.u.)
1.5
1.0
0.5
0.0
****
****
****
*
**
Control
Kk
GD
Kk+GD
dTBCE RNAi

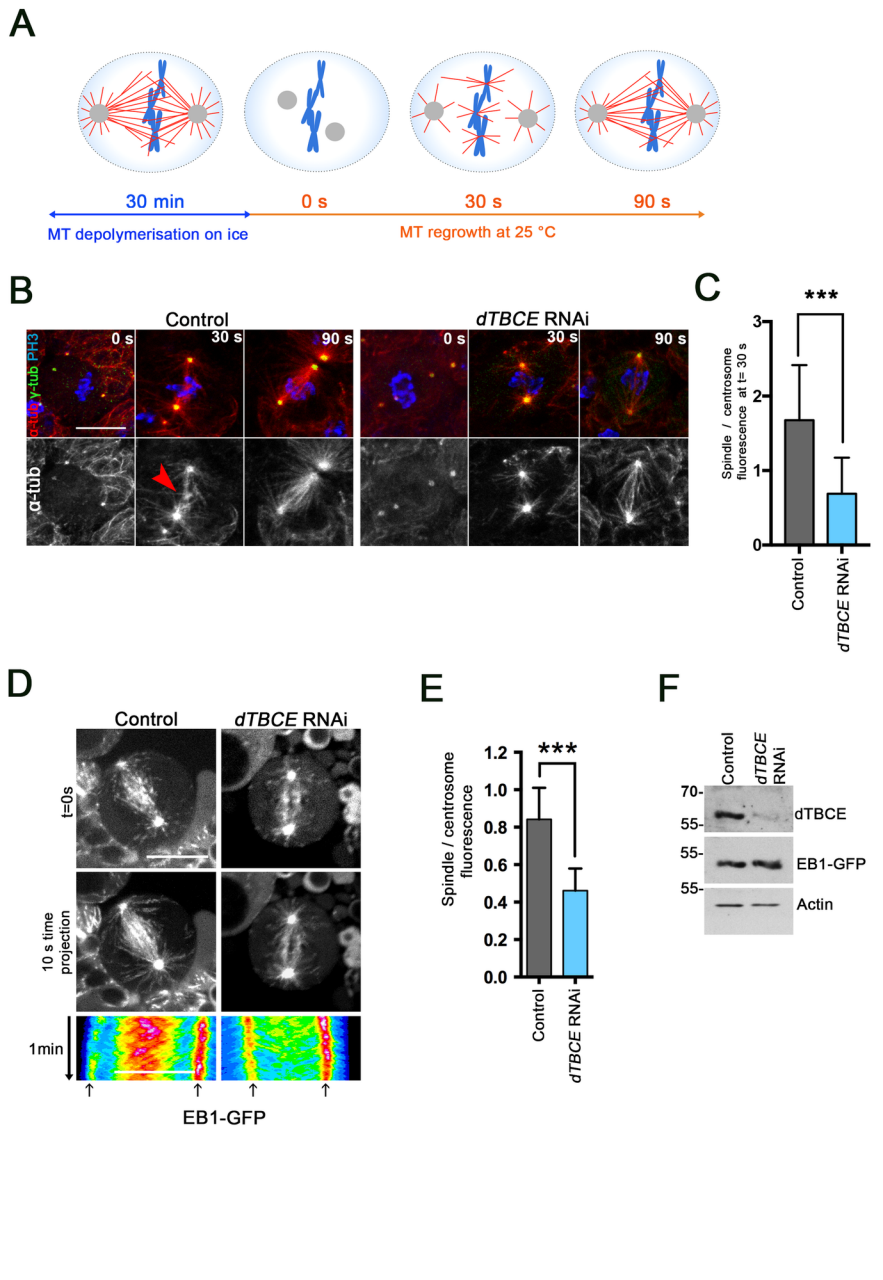
A
30 min
0 s
30 s
90 s
MT depolymerisation on ice
MT regrowth at 25 °C
B
Control
dTBCE RNAi
0 s
30 s
90 s
γ-tub PH3
α-tub
C
***
Spindle / centrosome fluorescence at t= 30 s
Control
dTBCE RNAi
D
Control
dTBCE RNAi
t=0s
10 s time projection
1min
EB1-GFP
E
***
Spindle / centrosome fluorescence
Control
dTBCE RNAi
F
Control
dTBCE RNAi
dTBCE
EB1-GFP
Actin

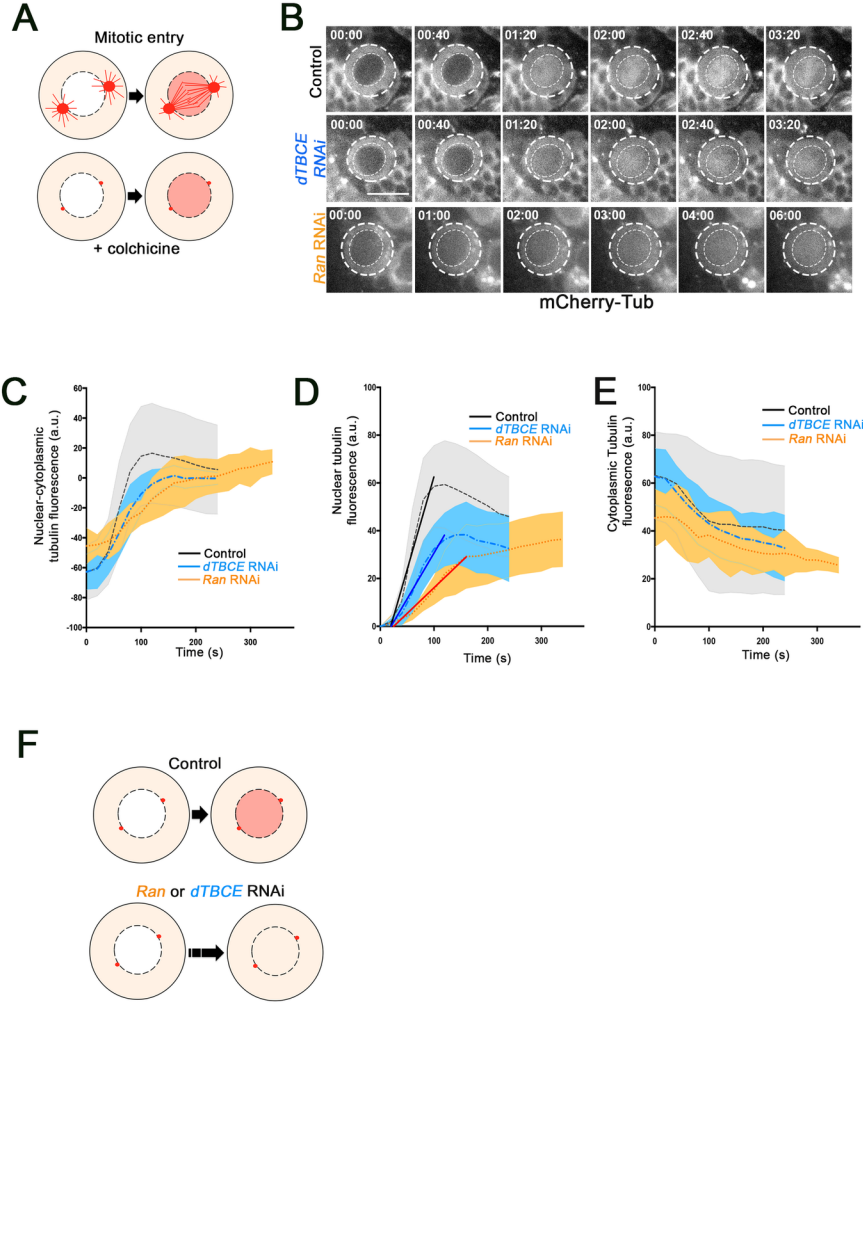
A
Mitotic entry
+ colchicine
B
Control
dTBCE RNAi
Ran RNAi
00:00
00:40
01:20
02:00
02:40
03:20
01:00
03:00
04:00
06:00
mCherry-Tub
C
Nuclear-cytoplasmic tubulin fluorescence (a.u.)
Time (s)
Control
dTBCE RNAi
Ran RNAi
D
Nuclear tubulin fluorescence (a.u.)
Time (s)
Control
dTBCE RNAi
Ran RNAi
E
Cytoplasmic Tubulin fluorescence (a.u.)
Time (s)
Control
dTBCE RNAi
Ran RNAi
F
Control
Ran or dTBCE RNAi

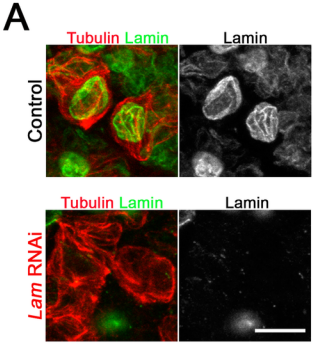
A
Tubulin Lamin
Lamin
Control
Tubulin Lamin
Lamin
Lam RNAi

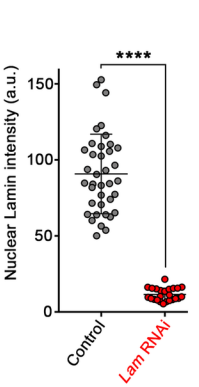
B
****
Nuclear Lamin intensity (a.u.)
150
100
50
0
Control
Lam RNAi

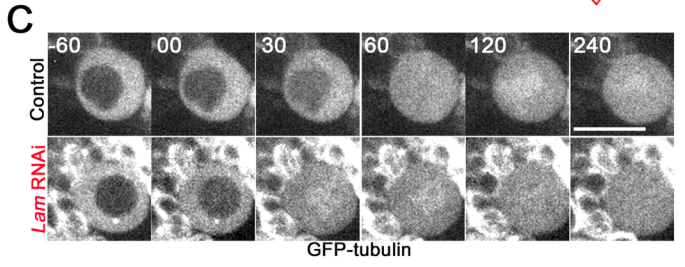
C
-60
00
30
60
120
240
Control
Lam RNAi
GFP-tubulin

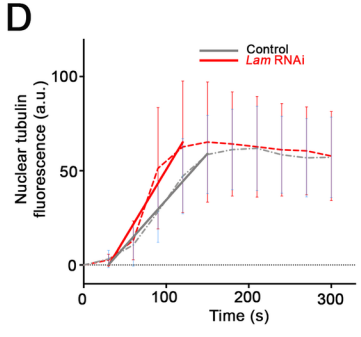
D
Control
Lam RNAi
Nuclear tubulin fluorescence (a.u.)
100
50
0
0
100
200
300
Time (s)

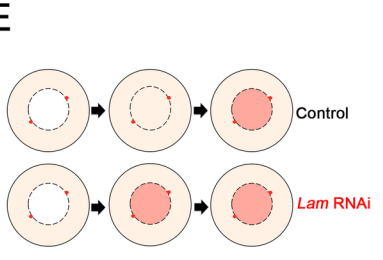
E
Control
Lam RNAi

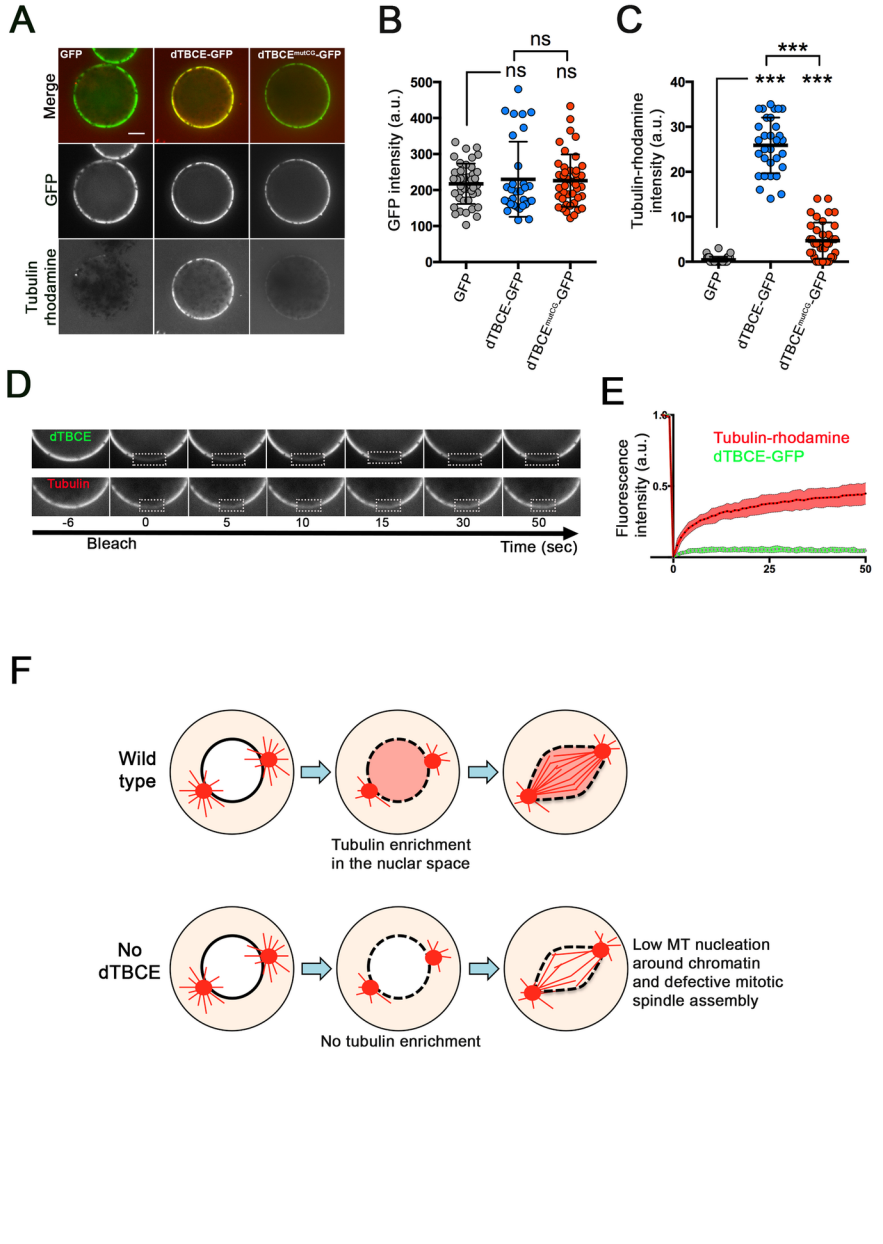
A
GFP
dTBCE-GFP
dTBCE^mutCG-GFP
Merge
GFP
Tubulin rhodamine
B
ns
ns
ns
GFP intensity (a.u.)
500
400
300
200
100
0
GFP
dTBCE-GFP
dTBCE^mutCG-GFP
C
***
***
***
Tubulin-rhodamine intensity (a.u.)
40
30
20
10
0
GFP
dTBCE-GFP
dTBCE^mutCG-GFP
D
dTBCE
Tubulin
-6
0
5
10
15
30
50
Bleach
Time (sec)
E
Fluorescence intensity (a.u.)
1.0
0.5
Tubulin-rhodamine
dTBCE-GFP
0
25
50
F
Wild type
Tubulin enrichment in the nuclar space
No dTBCE
No tubulin enrichment
Low MT nucleation around chromatin and defective mitotic spindle assembly

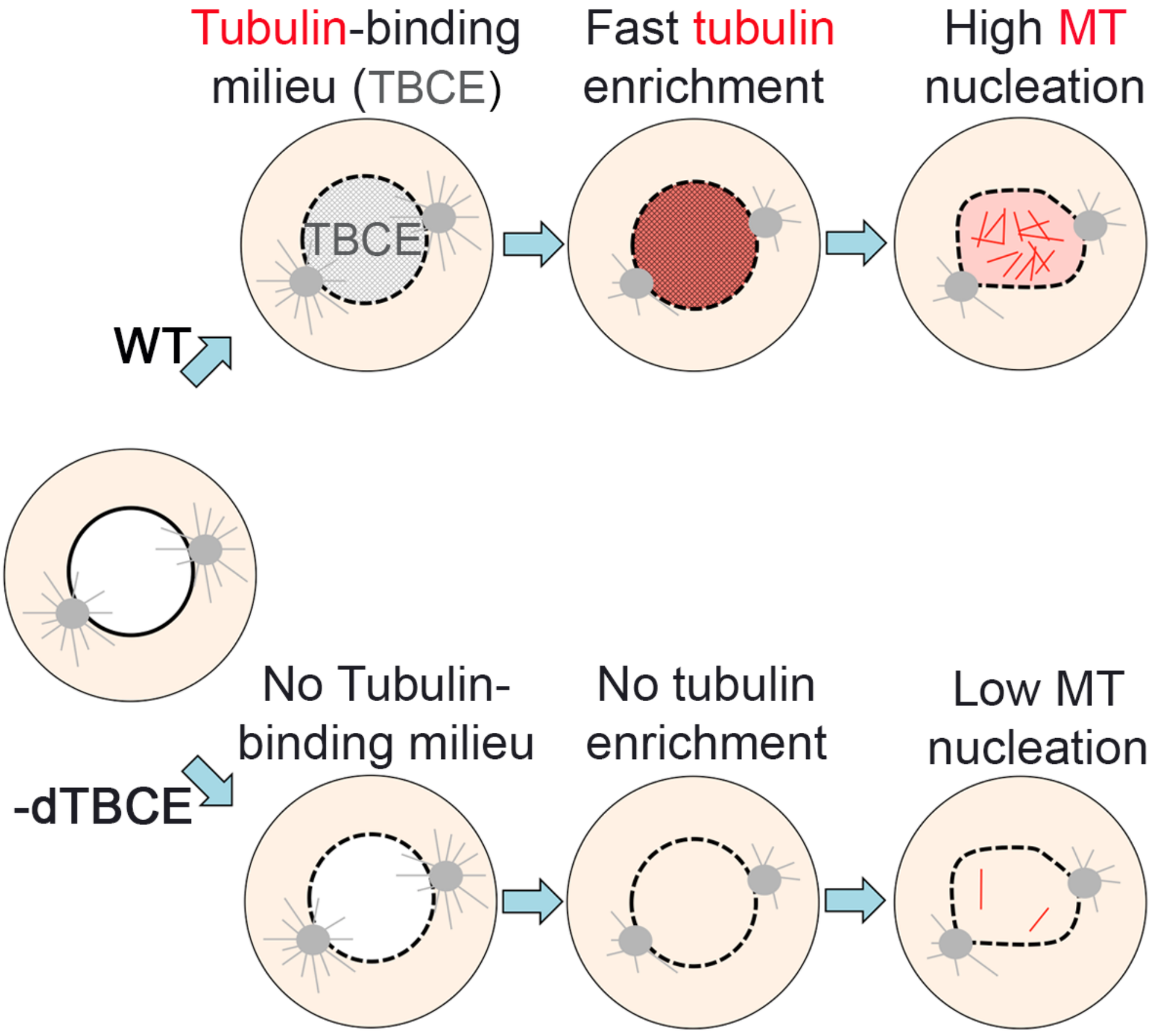
Tubulin-binding milieu (TBCE)
Fast tubulin enrichment
High MT nucleation
TBCE
WT
No Tubulin-binding milieu
No tubulin enrichment
Low MT nucleation
-dTBCE